HAPEX-Sahel

Basic description of methods and data sets

M. Soet, P. Droogers, M.N. Jaarsma, C.P. Kim, J.F. Monincx en J.N.M. Stricker

Funded by E.C. under contract EV5V-CT91-0033

RAPPORT 43

December 1993

Vakgroep Waterhuishouding
Nieuwe Kanaal 11, 6709 PA Wageningen

ISSN 0926-230X

CONTENTS

LIST OF FIGURES

LIST OF TABLES

1 INTRODUCTION

The Hydrological Atmospheric Pilot EXperiment in the Sahel (HAPEX-Sahel) is developed to improve the understanding of interactions between the land surface and the atmosphere in semi-arid areas. Similar programs have already been implemented in temperate areas, like HAPEX-MOBILHY in France, 1986, Fife in USA, 1987/1988 and for a semi-arid region EFEDA in Spain, 1991. HAPEX-Sahel includes an intensive field experiment from August 15 to October 9 1992 (Special Observation Period, SOP) and longterm extensive monitoring of soil and weather characteristics as rainfall and soil moisture. A comprehensive dataset was collected this way, which is useful for calibration and validation of upscaling techniques for general circulation models.
The observations covered an area of 100 km * 100 km in the Sahelian region of West-Africa, in Niger near the capital city Niamey. This area was chosen because it was well representative for the Sahelian zone and offered advantages considering infrastructure and available facilities. The intensive field experiment started at the end of the rainy season and lasted during part of the dry-down period, thereby including the transition from wet to dry soil conditions. During the SOP observations have been made at three representative supersites, each with an area of approximately 10 km * 10 km, within the larger domain of the experiment. For further information of the experiment, area characteristics and contributors, see the Experiment Plan for HAPEX-Sahel (Goutorbe et al., 1992).
The Department of Water Resources of the Agricultural University Wageningen was one of the contributors operating in the West-Central Supersite. The measurements were restricted to hydrological processes at and beneath the soil surface and were carried out to meet the following objectives:

- to monitore local waterbalances and hydrologic processes at different spatial scales,
- to characterize soil hydraulic properties and their spatial variability,
- to measure water content in the surface layer for calibration of remote sensing observations

To meet the objectives, the experimental effort during the SOP was divided into a monitoring part and a process-specific part and covered selected subsites in the West-Central Supersite with different kinds of vegetation and land-use (Table 1 and Fig. 1). The monitoring part included the collection of time-series of specific soil variables as soil moisture content and soil water suction. Therefore, plots were installed in the different subsites (except tiger-bush) to monitore soil moisture content every other day during the SOP. In addition, at several selected standard plots the soil water suction was measured every other day as well. The soil moisture content was also monitored extensively before and after the SOP. At the degraded bush subsite, a micro-catchment of 0.54 hectare was selected and surface runoff during and after rainfall was measured.
The process-specific data collection included measurements of in situ hydraulic conductivity at all subsites (except grassland) and characterization of overland flow by rainfall simulation at the degraded bush site. These processes were expected to be strongly influenced by the surface characteristics which varied from relatively loose and sandy to eroded with crust-formation after rainfall.
In addition, undisturbed soil samples were taken in gridpattern or in transects at different depths. These samples were used to determine the soil hydraulic properties in the

laboratory at WAU. To support remote sensing activities, the surfacial water content was measured on several days. Finally, efforts have been made to quantify soil evaporation by use of micro-lysimeters and at some days soil temperature and soil moisture were measured simultaneously in a single soil profile.

Table 1: Subsites West-Central Supersite

subsite	plotnr.	standard plot	vegetation
a	21-32	21,22,24,32	fallow bush
a'	41-44	42,44	grassland
b	1-10	1,3,4,8	millet
c			tiger bush
d	51-64	52,56,61,63	degraded bush

This report documents the field-activities and the resulting datasets. For that reason, the depicted results are hardly analyses. The first part of this report describes the set-up and methods used to determine the different characteristics. In the second part the data are described and some preliminary results are given. All data-sets, described in appendix II, are also available on diskette. In addition to this report, slides and photographs from the SOP are available.

This contribution is the result of enthusiastic and dedicated teamwork during and after the HAPEX-Sahel field experiment. This team consisted of the following persons (in alphabetical order): Peter Droogers, Marijke Jaarsma, René Kim, Sjon Monincx, Margje Soet and Han Stricker. Apart from the team-members mentioned, full support was given by the mechanical and electronic workshops of the Department in preparing the equipment. Logistic support during the field campaign was smoothly offered by the secretary-office.

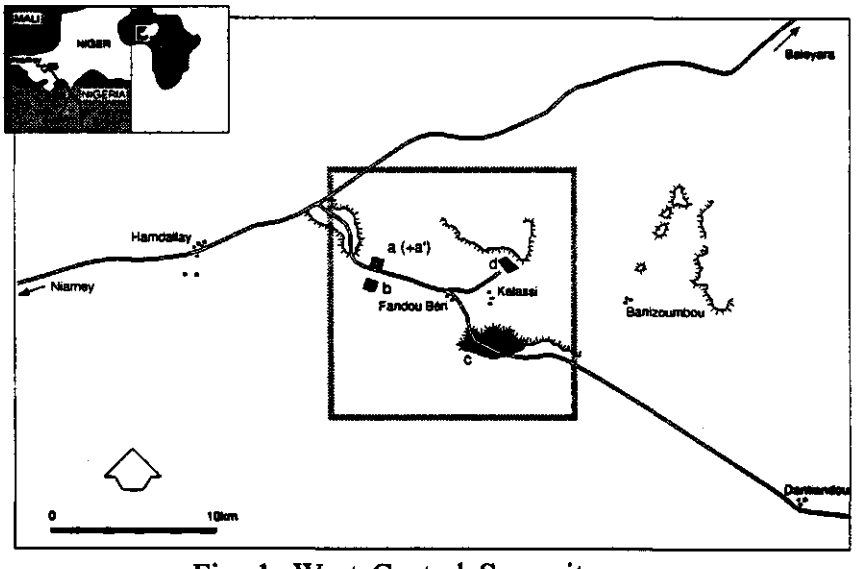

Fig. 1: West Central Supersite

2 MATERIALS AND METHODS

2.1 SOIL MOISTURE

Moisture content measurements at regular intervals were made at subsites fallow bush (a), grassland (a'), millet (b) and degraded bush (d), using a CPN neutron probe and Time Domain Reflectometry (TDR). In total 40 neutron probe access tubes (plots) were installed to a depth of 180 cm. Measurements were made at the 15, 25, 35, 45, 60, 75, 95, 115, 135, 155 and 170 cm depth. Fourteen of these plots were defined as standard plots (Fig. 2). The access tube was surrounded by TDR-probes in triplo at depths of 5, 10 (horizontal), 20-30 and 40-50 cm (vertical). The layout for each subsite is shown in Fig. 3 a-d. Neutron probe and TDR-measurements were generally made every other day during the SOP. However, after rainfall, extra measurements were taken. After the SOP, neutron probe measurements were continued on a monthly base so that information on long term processes becomes available.

Only data collected during the SOP at the West Central Supersite are presented in this report. A data-set with the longterm neutron probe measurements, collected in a more northern area near Ouallam, was reported separately (Monincx, 1993).

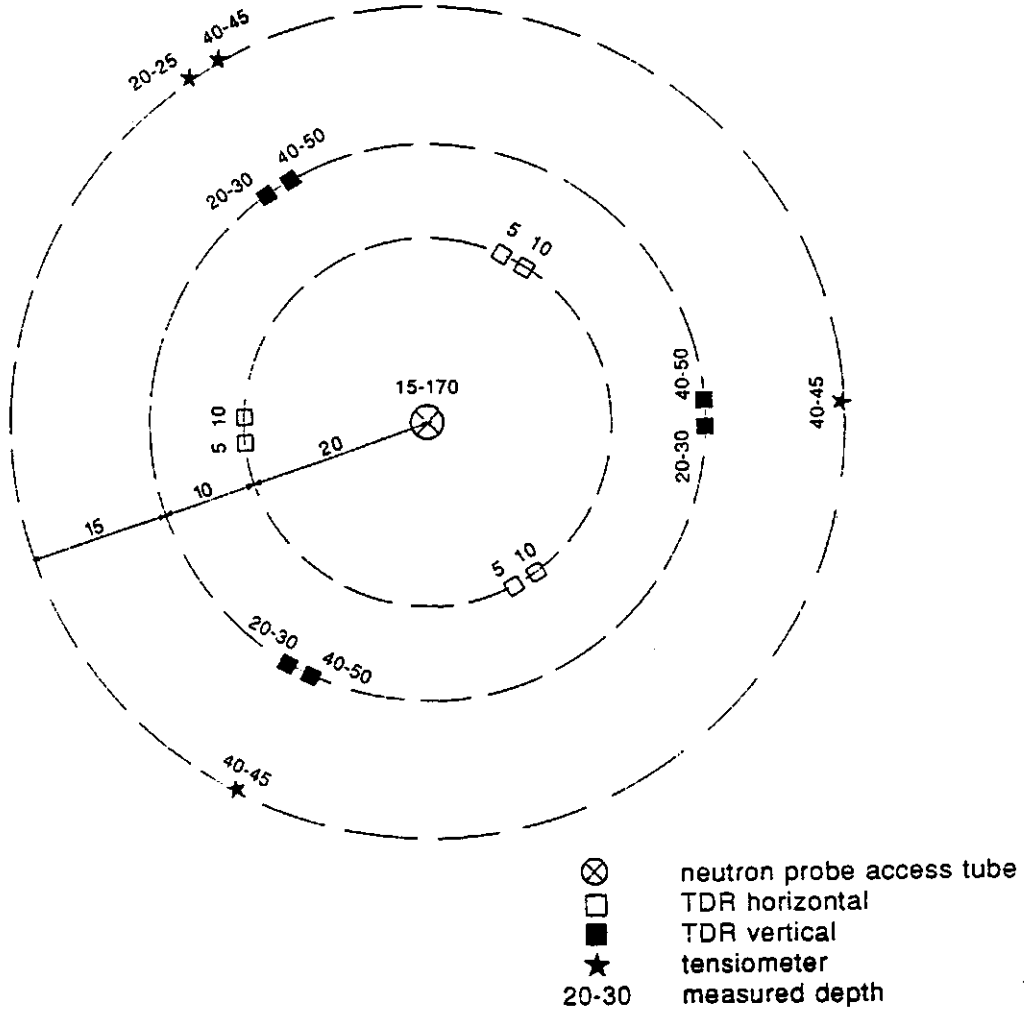

Fig. 2: Lay-out of a standard-plot

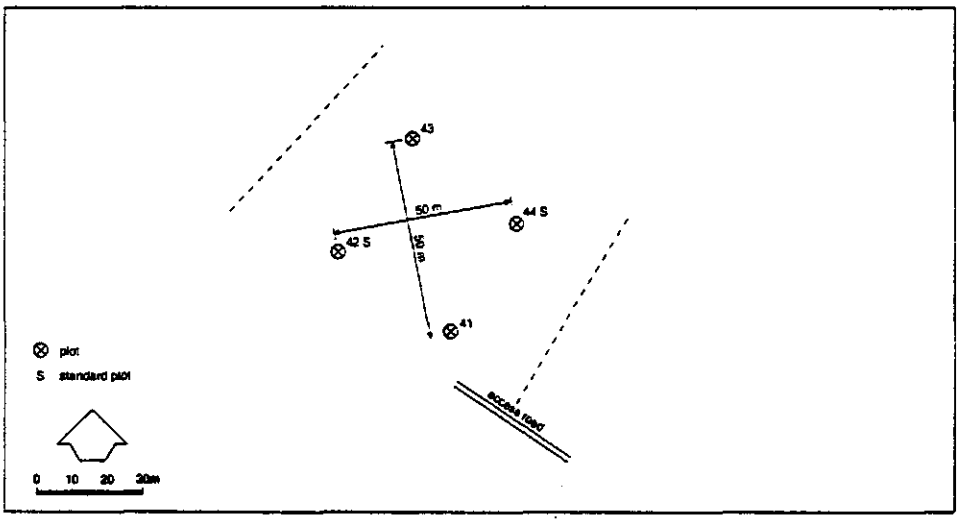

Fig. 3a: subsite grassland (a')

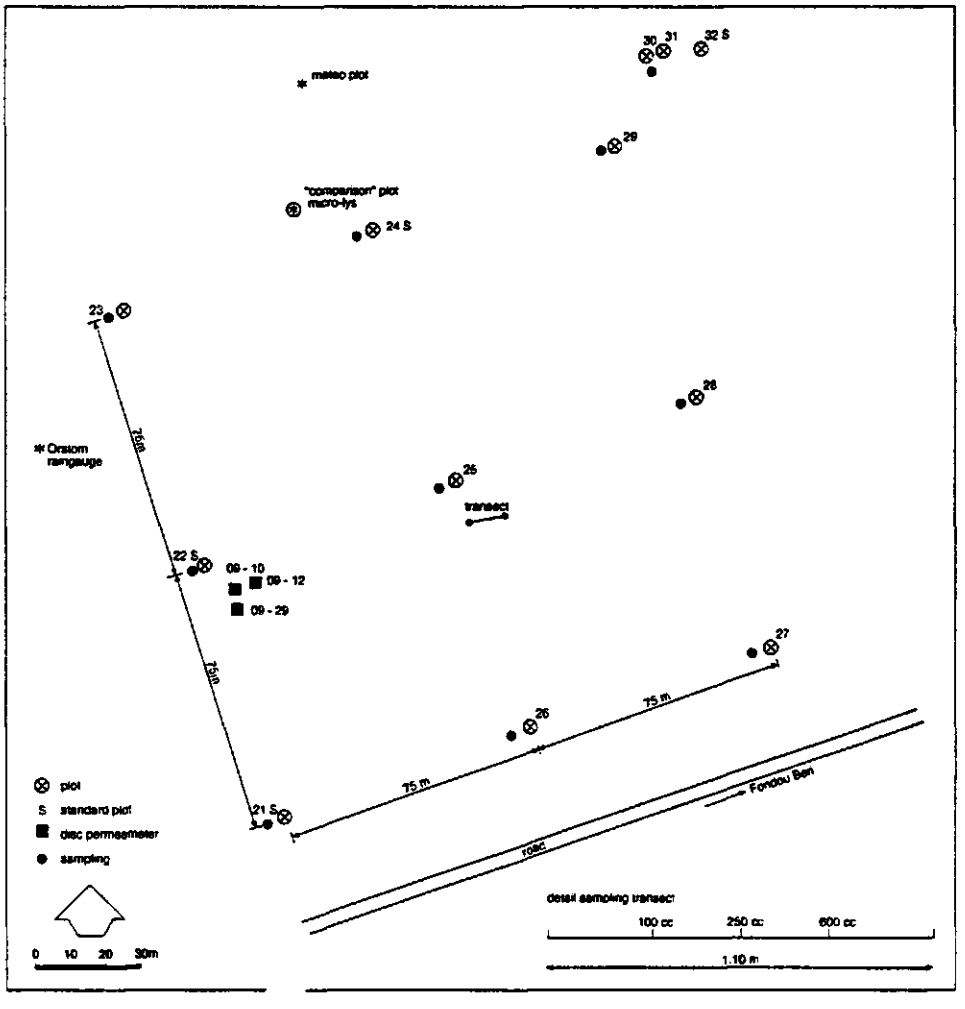

Fig. 3b: subsite fallow bush (a)

Fig. 3: lay-out of neutron probe access tube grids

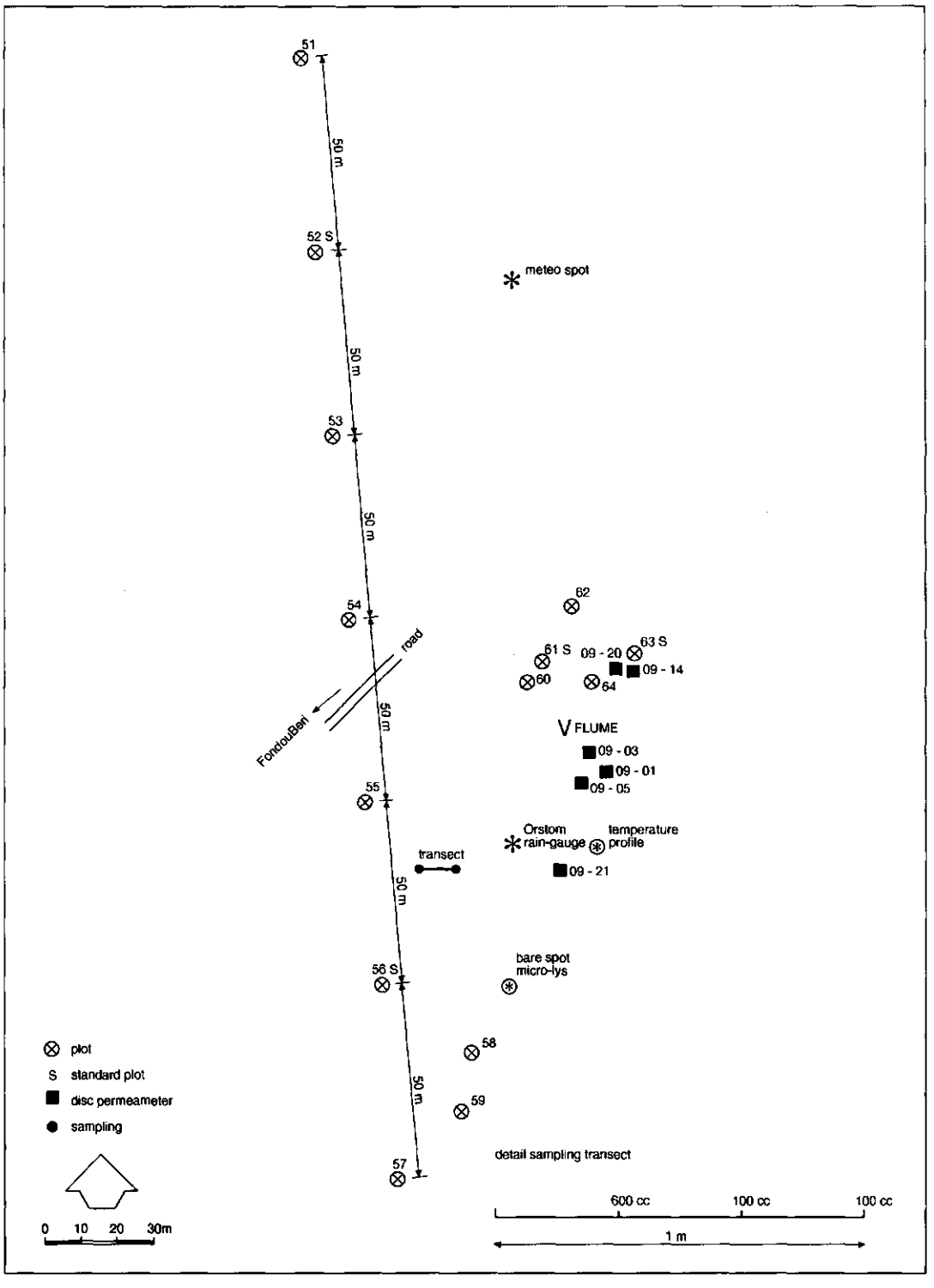

Fig. 3c: subsite degraded bush (d)

Fig. 3: lay-out of neutron probe access tube grids

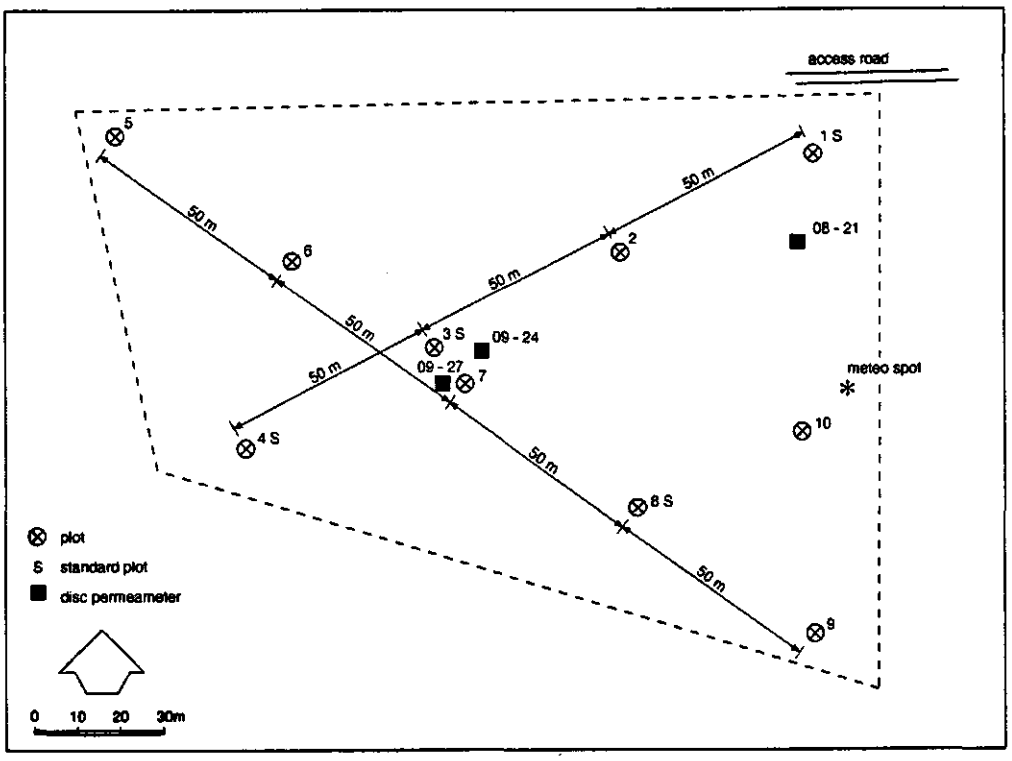

Fig. 3d: subsite millet (b)

Fig. 3: lay-out of neutron probe access tube grids

2.1.1 Neutron probe

Fast neutrons, emitted into soil from a radioactive source, are reduced in energy, predominantly by hydrogen. Therefore the number of detected low-energy neutrons is related to the moisture content of the surrounding soil volume. In order to calculate the moisture content from countnumber, the probe has to be calibrated for a particular soil. Neutron probe data are commonly presented as the number of counts divided by a number of counts in a standard medium. This count ratio is calibrated versus the independently measured soil moisture content, thereby yielding a linear, soil dependent relationship for the water content range of interest. In our case every day standard counts were made in water. As the standard counts did not change significantly during the meant period, the average standard count was used to calculate count ratios. The counting time was generally 16 seconds, but during several weeks in August also 64 or 32 seconds counting times were used. Table 2 shows there is little or no difference in the mean and a relatively small increase in C.V. (coefficient of variation) if counting time was reduced to 16 seconds.

Table 2: Comparison of counting time 16 and 32 seconds

	number of measurements	avg counts 32 sec	avg counts 16 sec	C.V. 32 sec	C.V. 16 sec
plot 42 depth 135 cm	15	5899	5899	0.009	0.011
standard medium (water)	10	22469	22505	0.003	0.007

Neutron probe measurements at 25 and 45 cm depth were calibrated against TDR-measurements at 20-30 cm and 40-50 cm depth. For each measured count ratio n at a standard plot there are 3 TDR-measurements of the moisture content, θ, at the same depth, surrounding the access tube at a distance of 30 cm. Thus a sampling error for moisture content θ could be estimated but not for n. Therefore, the most accurate calibration will be found when using a linear regression of n on θ, correcting for bias in θ.

The appropriate model for N (n_i', θ_i') pairs and R replicates of θ_{ij} is now (Greacen, 1981):

$$n_i' = n_i + \varepsilon_i = \alpha + \beta\theta_i + \varepsilon_i \tag{1}$$

$$\theta_{ij}' = \theta_i + \delta_{ij} \qquad i=1..N,\ j=1..R \tag{2}$$

$$var(\varepsilon_i) = \sigma_\varepsilon^2 \qquad var(\delta_{ij}) = \sigma_\delta^2 \tag{3}$$

with n_i': measured count ratio
n_i : true value
θ_i': measured volumetric moisture content
θ_i : true value

The estimators for α and β describing the calibration curve are:

$$b = \frac{s_{\bar{\theta},n}}{s_{\bar{\theta},\bar{\theta}} - \frac{1}{R}s_\theta^2} \qquad a = \bar{n}_\cdot - b\,\bar{\theta}_{\cdot\cdot} \tag{4}$$

in which $\frac{1}{R}s_\theta^2$ represents the extra term compared to classis linear regression.

The variances of ε_i and δ_{ij} are estimated by:

$$\hat{\sigma}_\delta^2 = s_\theta^2 \qquad \hat{\sigma}_\varepsilon^2 = s_{n,n}^2 - b\ c_{\bar{\theta},n} \tag{5}$$

where

$$s_\theta^2 = \frac{1}{N(R-1)} \sum_i^N \sum_j^R (\theta_{ij}' - \bar{\theta}_{i\cdot})^2 \tag{6}$$

$$s_{\bar{\theta},\bar{\theta}}^2 = \frac{1}{N-1} \sum_i^N (\bar{\theta}_{i\cdot} - \bar{\theta}_{\cdot\cdot})^2 \tag{7}$$

$$c_{\bar{\theta},n} = \frac{1}{N-1} \sum_{i}^{N} (\bar{\theta}_{i.} - \bar{\theta}_{..})(n_i' - \bar{n}) \qquad \text{and} \qquad (8)$$

$$s_{n,n}^2 = \frac{1}{N-1} \sum_{i}^{N} (n_i' - \bar{n})^2 \qquad (9)$$

with s_θ^2: variance of replicates
$s^2_{\theta,\theta}$: variance of means
$c_{\theta,n}$: covariance
$s^2_{n,n}$: variance of count ratios

Using this unbiased regression model, a calibration curve has been determined for each subsite (a+a', b and d). The estimators were calculated using data at the 25 cm depth only, at the 45 cm only and for combined data of both depths. The results showed that the error of estimated moisture content using the combined calibration curve is not significantly bigger than when using the single depth data (Fig. 4 a-c for the three subsites). Therefore, the combined curves were used. Final curves, values of calibration coefficients and variances are given in Fig. 5 a-c and Table 3.
It appears that the relatively large 95%-confidence interval at the degraded bush site is caused by the larger bias in θ, compared to the other subsites.

Table 3: Calibration coefficients neutron probe

subsite	a	b	N	σ_ε^2	σ_δ^2
fallow bush	0.027	1.88	317	1.2 E-3	8.08 E-5
millet	0.051	1.87	206	2.3 E-3	3.99 E-5
degraded bush	0.057	1.76	232	3.9 E-3	3.19 E-3

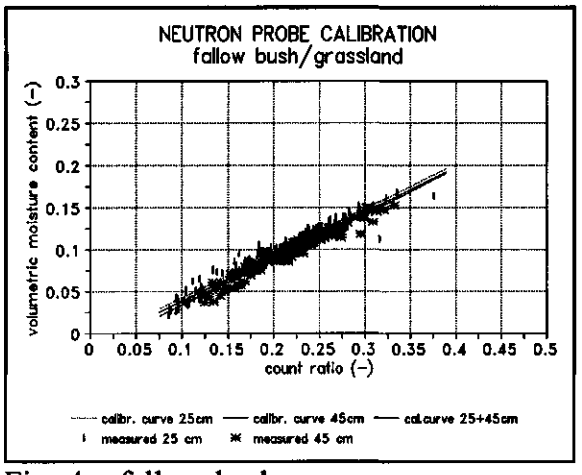

Fig. 4a: fallow bush

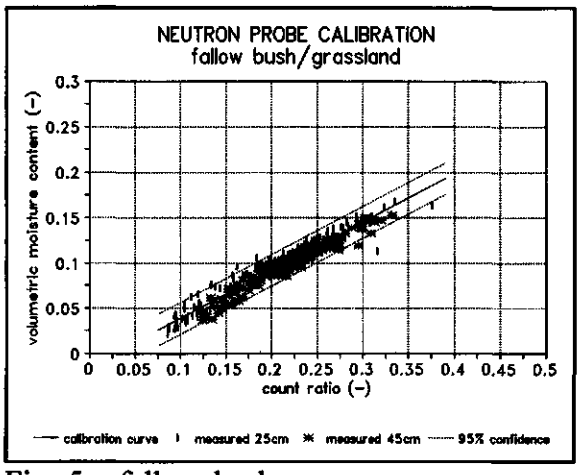

Fig. 5a: fallow bush

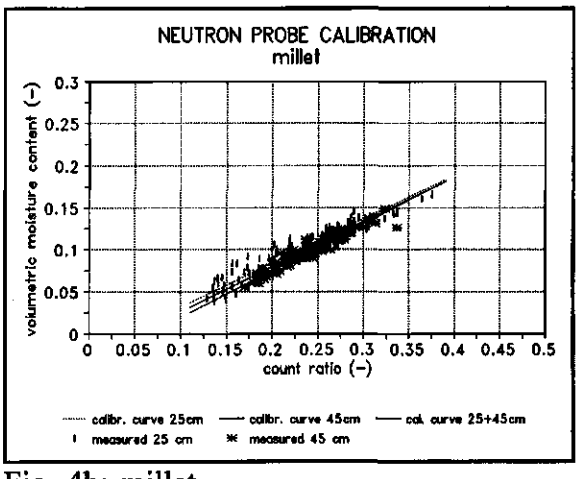

Fig. 4b: millet

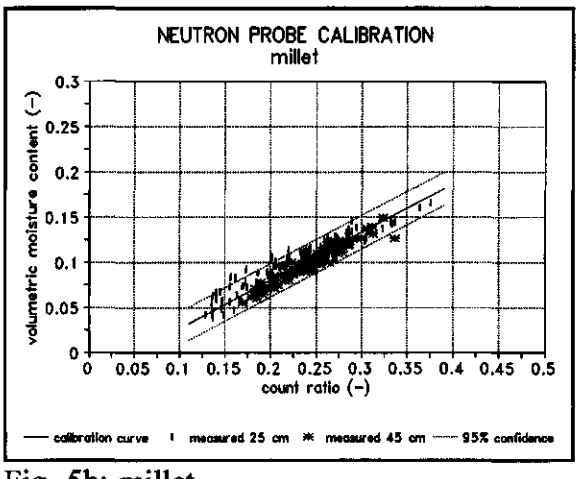

Fig. 5b: millet

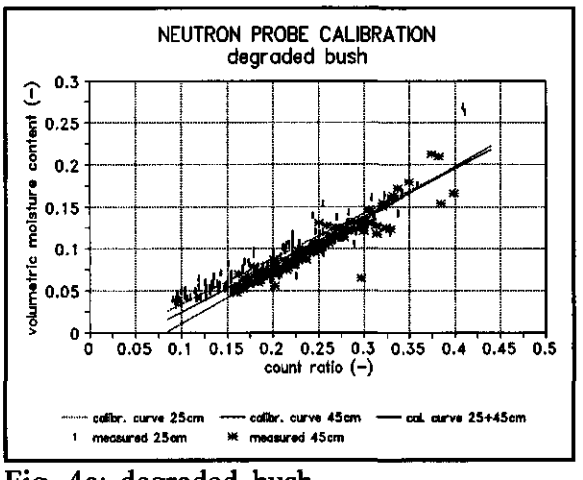

Fig. 4c: degraded bush

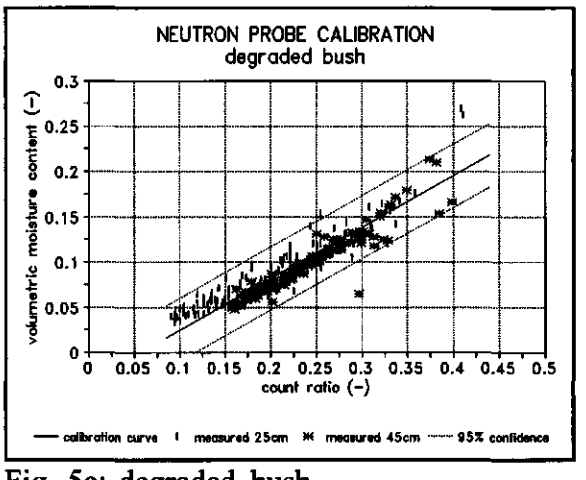

Fig. 5c: degraded bush

Fig. 4: calibration neutron probe single and combined depths

Fig. 5: final calibration curve neutron probe

2.1.2 Time Domain Reflectometry

TDR measurements are based on the difference in dielectric constants of water (80), air (1) and soil particles (≈ 4). An electro-magnetic impulse is transmitted into the soil along a probe. At the end of the probe the signal is reflected back to the instrument, where its return is recorded. Then the dielectric constant, ε_s, of the bulk soil can be calculated from (Roth et al., 1990):

$$\varepsilon_s = [(c_0 t) / (2L)]^2 \quad (10)$$

with c_0: speed of light in vacuum (m/s)
t: travel time of TDR signal (s)
L: length of the probe (m)

Measurements were made using 3 instruments: a cable-tester (CT) in combination with automatic waveform analysis (Heimovara, 1990) and 2 systems of Easy Test Ltd (FOM/m and FOM/mts) that display directly moisture contents through known, internal conversion of measured travel times. However, the automatic analysis was not accurate. Thus, a separate calibration was done in the laboratory to obtain identical dielectric constant ε values for all three instruments. The calibration concentrated on the dry range of moisture contents, resembling field conditions.

For the calibration, 14 undisturbed samples were taken from different subsites and, in order to get information in the very dry range, 9 additional samples were packed in the laboratory with porosity equal to undisturbed samples. Both the undisturbed and samples were PVC-rings with a diameter of 8 cm and a length of 12 cm (except for 3 samples collected in an iron ring).
In the middle of these samples, a 10-cm length two-rod TDR sensor was placed and travel-time (CT) or volumetric moisture content (FOM/m, FOM/mts) was measured, without removing the TDR-sensor. The volumetric moisture content of the samples was obtained by oven drying (undisturbed samples) or calculated from a fixed volume of water mixed with a known mass of dry soil (packed samples). For each sample three dielectric constants were calculated from travel time for CT or by using the built-in calibration curve of the instrument for FOM/m and FOM/mts.
Since the dielectric constant given by CT is chosen as a reference for FOM/m and FOM/mts, a fitting procedure was done to get identical dielectric constants. The curves are described by equations (12) and (13) and are shown in Fig. 6 a and b.

$$\varepsilon_{cal}(MTS) = -0.00144\varepsilon_{mts}^3 + 0.0663\varepsilon_{mts}^2 + 0.1288\varepsilon_{mts} + 2.213 \quad (11)$$

$$\varepsilon_{cal}(M) = -0.00192\varepsilon_m^3 + 0.0576\varepsilon_m^2 + 0.4301\varepsilon_m + 1.311 \quad (12)$$

where ε_{mts} and ε_m are the original values as computed by internal conversion and ε_{cal} are the corrected values of the FOM/mts and FOM/m instrument. Note that in this procedure ε_{cal} corresponds with ε_{CT}, being the reference.

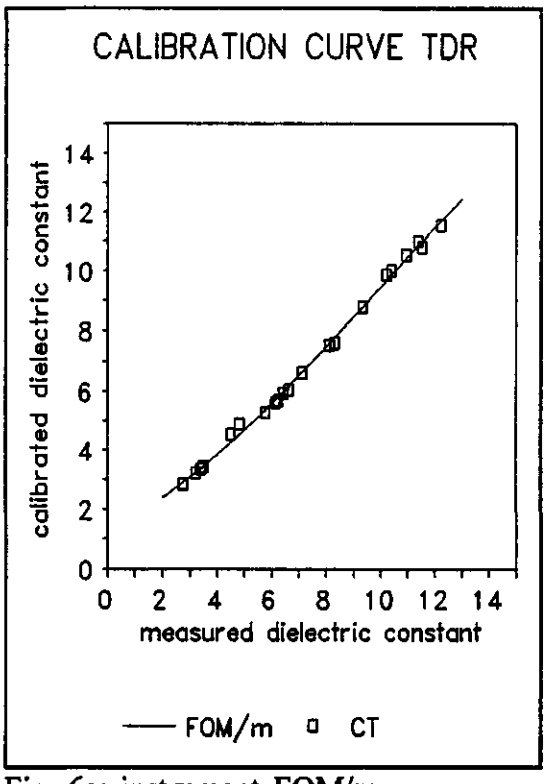

Fig. 6a: instrument FOM/m

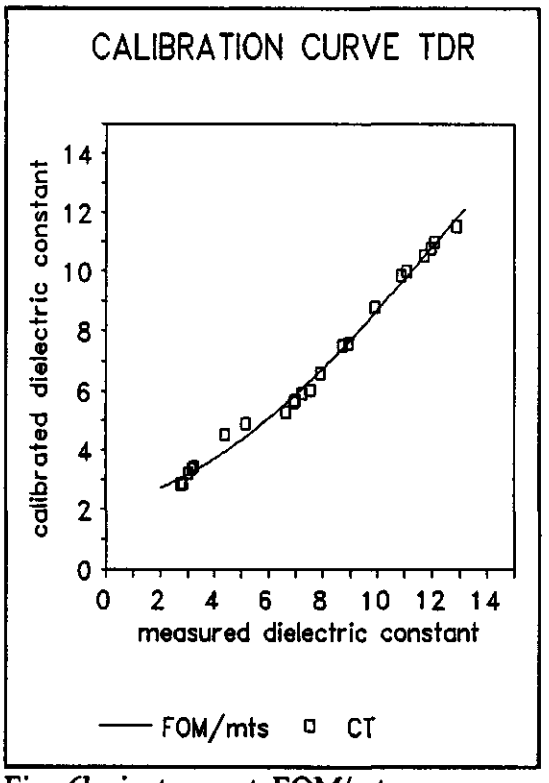

Fig. 6b: instrument FOM/mts

Fig. 6: Calibration curves for dielectric constant of TDR-instruments

Finally, the dielectric constant ϵ_{cal} was calibrated versus the volumetric moisture content obtained by oven drying:

$$\theta(\varepsilon_{cal}) = 0.000308\varepsilon_{cal}^3 - 0.0076\varepsilon_{cal}^2 + 0.0811\varepsilon_{cal} - 0.1732 \qquad (13)$$

The calibration curve is presented in Fig. 7 and compared to the calibration curve derived by Topp et al. (1980). The moisture contents calculated using the Topp-curve would cause errors in the important dry range ($\theta \leq 0.08$).
Standard deviation and regression coefficient R^2 of the definite calibrated and measured moisture contents are given in Table 4.

Table 4: Statistical evaluation of calibrated versus measured watercontents based on 23 observations of 23 samples

instrument	maximum error in calculated θ	standard deviation	R^2
cable-tester	0.012	0.0070	0.990
FOM/m	0.019	0.0094	0.983
FOM/mts	0.014	0.0071	0.990

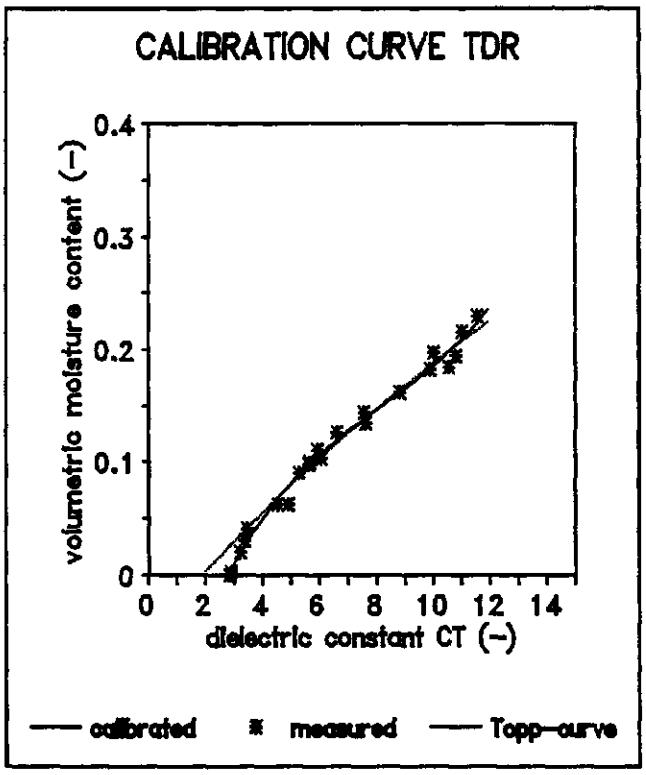

Fig. 7: Calibration curve of volumetric moisture content TDR

2.2 SOIL WATER SUCTION

At all standard plots tensiometers have been installed in order to measure soil water suction. The tensiometers were installed vertically with the ceramic cup at a depth of 20-25 cm (1x) and 40-45 cm (3x). The measurement-device consisted of a syringe needle, attached to a pressure transducer with digital read-out. For each measurement the needle was inserted through a septum stopper, which sealed the upper end of the tensiometer after withdrawal of the needle (Marthaler et al., 1983).

Above a suction of approximately 800 cm the suction measurements with tensiometry were invalid because of dissolution of gases from the water. In this case tensiometers were refilled in the field after rainfall. Septums were replaced if slow leakage occured due to repeated insertion.

2.3 CATCHMENT

At the degraded bush subsite a mini-basin was selected to study the relationship between rainfall and surface-runoff during the SOP. The catchment was partly vegetated and partly eroded. The eroded area was bare with a thin surface crust. The catchment was equiped with a nearby raingauge (EPSAT) and a flume combined with an automatic recording system registrating the water head once per minute. The flume was calibrated in the laboratory, yielding:

$$Q(h) = 0.1396h^2 - 0.1985h + 1.6479 \quad h \geq 5 \text{ cm} \qquad (14)$$
$$Q(h) = 0.2846h^{1.6643} \quad h < 5 \text{ cm}$$

with Q: flow rate (l/s)
h: water head (cm)

Five plots were chosen for soil moisture monitoring (of which two were standard plots) Downwind of the catchment, energy balance measurements were carried out by the 'Berlin'-group (see also Fig. 3d and appendix I).
A topographic field survey was made to determine the area contributing to runoff. The resulting elevation map is shown in Fig. 8, including the catchment border. The total catchment area was 5380 m^2.

2.4 IN SITU HYDRAULIC CONDUCTIVITY

2.4.1 Theory

The hydraulic conductivity near saturation was measured in situ using a disc permeameter (see Fig. 9). Water is infiltrating into the soil from a surface disc which supplied water under a negative pressure ψ. Wooding (1968) analysed the three-dimensional flow from a shallow circular pond or surface disc and showed that, for a homogeneous, isotropic soil under uniformly unsaturated initial conditions, the steady state volumetric flow rate Q from the circular source is given by:

$$Q = \pi r^2 K(\psi) + 4r\Phi(\psi) \qquad (15)$$

The matrix flux potential Φ is described by (Gardner, 1958):

$$\Phi(\psi) = \int_{\psi_0}^{\psi} K(\psi) d\psi \qquad (16)$$

Q: steady infiltrating flux (m^3/s)
K: hydraulic conductivity (m/s)
r: source radius (m)
Φ: matrix flux potential (m^2/s)
ψ: soil water potential (m)
ψ_0: reference soil water potential (m)

While measuring time and infiltration rate, the unsaturated hydraulic conductivity can be determined by a number of different procedures. These procedures are described briefly hereafter.

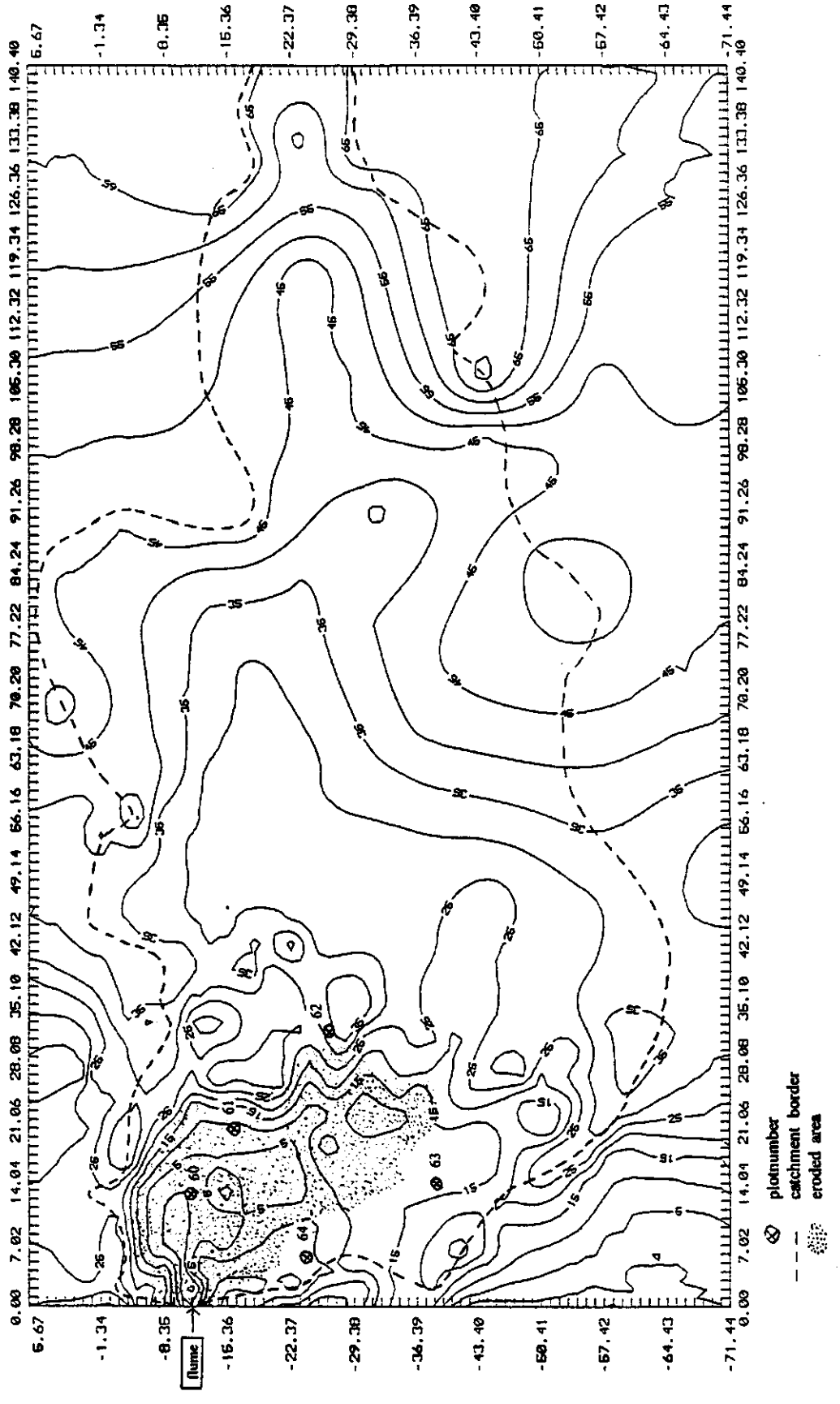

Fig. 8: Elevation map of the micro-catchment at the degraded bush subsite

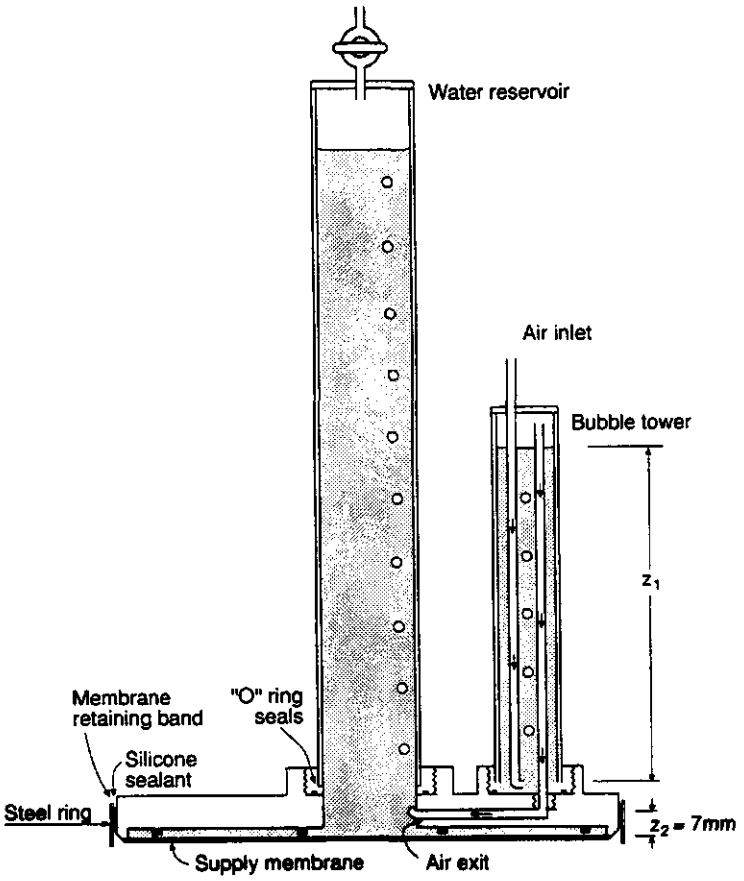

Fig. 9: The disc permeameter apparatus

1. Sorptivity

Wooding's solution for steady state infiltration from a circular source can be rewritten as (Smettem & Clothier, 1989):

$$Q = \pi r^2 K(\psi) + 4r\frac{bS^2}{(\theta_n - \theta_i)} \qquad (17)$$

θ_n: moisture content at supply potential (-)
θ_i: initial moisture content (-)
S: sorptivity ($m/s^{1/2}$)
b: dimensionless constant $1/2 < b < \pi/4$

During the early stages of the flow from the disc, the flow process is dominated by capillarity and cumulative infiltration is given by:

$$\frac{Q_{cum}}{\pi r^2} = St^{1/2} \qquad (18)$$

Q_{cum}: total volume of water infiltrated (m^3)
t: time from start of infiltration (s)

Plotting cumulative infiltration versus square root of time, the sorptivity is estimated as the slope of the straight line at the early measurement times.
In order to calculate the hydraulic conductivity, the measurements required are sorptivity, steady state flow rate, initial volumetric moisture content and volumetric moisture content at the supply potential. The constant b is in general taken 0.55 for field soils. Then K can be determined as:

$$K(\psi) = \frac{Q}{\pi r^2} - \frac{4bS^2}{\pi r(\theta_n - \theta_i)} \qquad (19)$$

2. Multiple disc radii

Because the initial square-root-of-time behaviour only occurs over a short period, practical difficulties in measuring sorptivity can result. Smettem & Clothier (1989) and Thony et al. (1991) described an alternative method, where measurements are made at identical supply pressures with discs of different radii at nearby, but separate spots. For each disc radius the hydraulic conductivity can be determined separately:

$$K(\psi) = \frac{Q_1}{\pi r_1^2} - \frac{4bS^2}{\pi r_1(\theta_1 - \theta_{i1})} \qquad (20)$$

$$K(\psi) = \frac{Q_2}{\pi r_2^2} - \frac{4bS^2}{\pi r_2(\theta_2 - \theta_{i2})} \qquad (21)$$

Now the sorptivity can be eliminated from (20) and (21) and the only measurements required in order to determine the hydraulic conductivity are steady state flow rate, initial and final water content:

$$S = \left[\frac{1}{4b}\left(\frac{Q_1}{r_1^2} - \frac{Q_2}{r_2^2}\right)\left(\frac{r_1\Delta\theta_1 r_2\Delta\theta_2}{r_2\Delta\theta_2 - r_1\Delta\theta_1}\right)\right]^{1/2} \qquad (22)$$

$$K = \frac{Q_1}{(\pi r_1^2)} - \frac{1}{\pi}\left(\frac{Q_1}{r_1^2} - \frac{Q_2}{r_2^2}\right)\left(\frac{r_2\Delta\theta_2}{r_2\Delta\theta_2 - r_1\Delta\theta_1}\right) \qquad (23)$$

The main disadvantage of this method is, that measured steady state outflow rates and moisture contents are being compared for different soil surface areas, which may introduce influence of spatial variability.

3. Multiple supply potentials

Ankeny et al. (1991) and Reynolds & Elrick (1991) developed an alternative procedure for determining soil hydraulic conductivity from disc permeameter data. In both

procedures the hydraulic conductivity is determined from measuring the steady state outflow at different tensions at the same measurement site, using the same disc radius. Therefore, the measurements are less influenced by soil heterogeneity and initial and final water contents do not have to be measured.

3A. The procedure described by Ankeny et al. (1991) is based on measuring fluxes $Q(\psi_x)$ and $Q(\psi_y)$ at potentials ψ_x and ψ_y, yielding two forms of equation (15) and 4 unknowns:

$$Q(\psi_x) = \pi r^2 K(\psi_x) + 4r\Phi(\psi_x) \quad (24)$$

$$Q(\psi_y) = \pi r^2 K(\psi_y) + 4r\Phi(\psi_y) \quad (25)$$

Then they assume a constant $K(\psi)/\Phi(\psi)$ ratio throughout the pressure range ψ_x to ψ_y:

$$A = K(\psi) / \Phi(\psi) = \text{constant} \quad (26)$$

and approximate the difference between $\Phi(\psi_x)$ and $\Phi(\psi_y)$ by:

$$\Phi(\psi_x) - \Phi(\psi_y) = \Delta\psi \; [K(\psi_x)+K(\psi_y)] / 2 \quad (27)$$

with $\Delta\psi = \psi_x - \psi_y$, x = 1,2,3,... and y = x+1.

Substituting (26) into (24), (25) and (27) provides a system of three equations with three unknowns that can be solved simultaneously in order to calculate the hydraulic conductivity for a pair of infiltration rates at different supply pressures:

$$Q(\psi_x) = [\pi r^2 + 4r/A] \; K(\psi_x) \quad (28)$$

$$Q(\psi_y) = [\pi r^2 + 4r/A] \; K(\psi_y) \quad (29)$$

$$[K(\psi_x)-K(\psi_y)] / A = \Delta\psi \; [K(\psi_x)+K(\psi_y)] / 2 \quad (30)$$

In case several outflow rate pairs have been measured, each pair of rates yields a single estimate of the constant A and an estimate of $K(\psi)$ for each supply pressure. Ankeny et al. (1991) defined the best estimate of $K(\psi)$ as the arithmetic average of available estimates and used a separate value of A for each pair of supply pressures.

3B. The procedure derived by Reynolds & Elrick (1991) is based on Wooding's solution, rewritten as:

$$Q = \left(\frac{r}{G_d} + \pi r^2 \alpha\right) \Phi \quad (31)$$

The α-parameter is defined by (Gardner, 1958):

$$K(\psi) = K_{fs}\exp(\alpha\psi) \qquad \begin{matrix} 0<\alpha<\infty \\ -\infty<\psi\leq 0 \end{matrix} \tag{32}$$

G_d: dimensionless shape factor (= 0.25)
K_{fs}: field-saturated hydraulic conductivity (m/s)
α: soil texture/structure parameter (m^{-1})

If (32) is substituted into (16) then:

$$\begin{aligned} \Phi_n &= \frac{K_{fs}}{\alpha}\left[\exp(\alpha\psi_n)-\exp(\alpha\psi_i\right] \\ &= \frac{1}{\alpha}\left[K(\psi_n)-K(\psi_i)\right] \end{aligned} \tag{33}$$

Assuming $K_i << K_n$, equation (33) is approximated by $K(\psi_n)/\alpha$.

Substituting $\Phi_n = K(\psi_n) / \alpha$ into (30) and transforming logarithmically produces:

$$\ln Q = \alpha\psi_n + \ln\left[\left(\frac{r}{G_d\alpha}+\pi r^2\right)K_{fs}\right] \tag{34}$$

For real soils $\alpha \approx$ constant over small ranges of ψ. Therefore, Reynolds & Elrick (1991) therefore estimated K(ψ) over the range $-\infty < \psi \leq 0$ by a piece-wise exponential relationship:

$$K(\psi) = \overline{K_{x,y}}\exp(\overline{\alpha_{x,y}}\psi) \tag{35}$$

in which $K_{x,y}$ and $\alpha_{x,y}$ represent an average value of K and α over the range $\psi_{x\rightarrow y}$.

Rewriting (34) using this piecewise approach gives:

$$\ln Q = \overline{\alpha_{x,y}}\psi_n + \ln\left[\left(\frac{r}{G_d\overline{\alpha_{x,y}}}+\pi r^2\right)\overline{K_{x,y}}\right] \tag{36}$$

which describes a piecewise linear plot as shown in Fig. 10. The $\alpha_{x,y}$-parameter can be determined from the piecewise slope:

$$\overline{\alpha_{x,y}} = \frac{\ln(Q_x/Q_y)}{\psi_x-\psi_y} \tag{37}$$

and $K_{x,y}$ can be determined from the piecewise intercept:

$$\overline{K_{x,y}} = \frac{G_d \overline{\alpha_{x,y}} Q_x}{r(1 + G_d \overline{\alpha_{x,y}} \pi r)(Q_x/Q_y)^P} \qquad (38)$$

with $P = \psi_x/(\psi_x-\psi_y)$.

An estimate of $K(\psi)$ is obtained by substituting (37) and (38) into (35). In case several outflow rate pairs have been measured, two estimates of $K(\psi_n)$ can be obtained for each ψ_n, that can be averaged to yield one $K(\psi_n)$ estimate. A more appropriate approach may be to estimate $K(\psi_{x,y})$, where $\psi_{x,y}=(\psi_x+\psi_y)/2$.

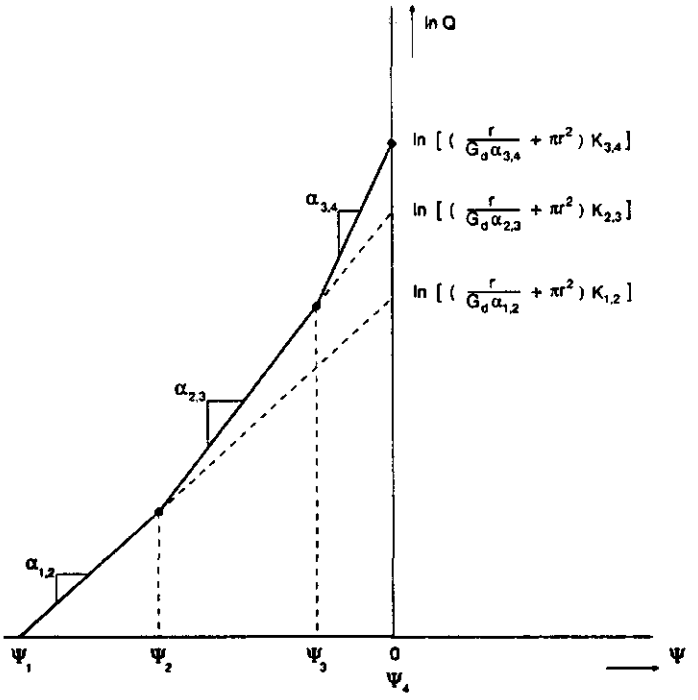

Fig. 10: Piece-wise linear relationship of steady state flowrate versus supply-pressure

2.4.2 Measurements

The method of measuring at multiple supply potentials on the same soil surface has been chosen to determine the in situ hydraulic conductivity of several locations in the different subsites. The infiltration is expected to be strongly influenced by the existence of a surface crust, covering a large extent of the soil surface in the area. Different types of crusts can be distinguished according to a classification by Casenave & Valentin (1989). Different crust types are classified depending upon their formation. A structural crust (ST) is mainly caused by raindrop impact, resulting in a thin compacted layer with coarser particles on top of finer ones. After the coarse particles on top are removed by erosion, a rigid, thin layer of fine particles was defined as an erosion crust. In each subsite measurements were made on crust type, most typical of that area. These are given in Table 5.

At each spot in situ K-measurements were made both at the surface and at some

centimeters below the surface after careful removal of the crust. At the conclusion of both measurements, 2 soil samples of 100 cc were taken directly under the disc. The hydraulic properties of these samples were determined in the laboratory by the multi-step outflow method.
For measurements at subsite c (tigerbush) it was impossible to remove the crust without disturbing the subsurface. Therefore only measurements at the surface were made and soil samples were not taken. In the Northern Satellite site was no distinct surface crust. Therefore no separate measurements below the surface were taken.
Infiltration measurements were started at a supply pressure of -11 cm using 2 identical disc permeameters (A and B) with a disc radius of 9 cm. Before placing the disc permeameter on the surface, vegetation was carefully removed and a thin layer of sand was applied to establish good contact between the disc supply membrane and the soil. Thereafter, the disc permeameter at a tension of -11 cm was placed on the surface and time versus outflow were recorded for about 1 hour to ensure steady state flow. Then, the waterlevel in the bubble-tower was adjusted so that the tension at the supply membrane was about -8.5, -5.5, -2.5 and 0 cm successively. Steady state flow rates for these steps were rapidly reached ($\approx$ 10 minutes). In case the disc permeameter was removed during the experiment to refill the waterreservoir, it was replaced carefully at exactly the same location after restoring the contact layer.
The disc was surrounded by a sharpened metal ring, pushed about 0.5 cm into the soil (except for measurements made in subsite c). In this way, vertical flow through the crust can be assumed and instability of the disc permeameter due to strong wind was avoided. During the experiment the lower part of the disc permeameter was shaded in order to avoid errors caused by fluctuations in water temperature.

In the East Central supersite disc permeameter measurements have been made by the "Institut de Mécanique de Grenoble", according to the method of Thony et al. (1991) using multiple disc radii. In order to make an intercomparison of both methods simultaneous measurements within an area of about 5 m^2 were made in the East Central supersite, subsite tigerbush, and in the West Central supersite, subsite degraded bush.

Table 5: Typical crust types

(sub)site	crust type
fallow bush	erosion
	ST3
millet	erosion
	ST3
tigerbush	algea
	ST3
degraded bush	erosion
	ST3
Northern Satellite site	---

2.5 SOIL HYDRAULIC PROPERTIES

The multi-step outflow method to determine the soil hydraulic properties is a laboratory method. Undisturbed samples of 100 cc, 250 cc and 600 cc were taken in the field. In the laboratory, each sample was placed in a Tempe pressure cell on top of a ceramic plate (Fig. 11).

After saturating a sample from below, a small suction was applied until equilibrium was reached. Then the pneumatic pressure on top of the sample was increased, thereby inducing drainage of the soil sample while the ceramic plate remains saturated. This combined system of soil and ceramic plate has the following initial and boundary conditions (Van Dam et al., 1992):

$h = h_0(x)$	$t = 0$	$0 \le x \le L$
$\delta h/\delta x = 1$	$t > 0$	$x = 0$
$h = h_L - h_a$	$t > 0$	$x = L$

with x=0: top of soil core (cm)
L: height of sample + ceramic plate (cm)
h_L: initial water potential below ceramic plate (cm)
h_a: applied pneumatic pressure (cm)

During a period of about 2 weeks, the pressure on top of the sample was increased stepwise until a pressure of 1 bar was reached. During the experiment time and outflow were recorded.

Through application of a one-dimensional unsaturated flow model on the measured time-outflow data, hydraulic properties can be estimated by inverse modelling. This inverse method is based on the principle that the flow-process is repeatingly simulated with adjusted soil hydraulic properties until the simulated outflow is sufficiently close to the observed outflow. To derive soil hydraulic properties in this way, one has to use analytical functions to describe these properties. In this experiment the Mualem-Van Genuchten (MVG) model was used (Van Genuchten, 1980):

$$\Theta = [1+(\alpha|h|)^n]^{-m} \tag{48}$$

$$K = K_s \Theta^l [1-(1-\Theta^{1/m})^m]^2 \tag{49}$$

where $\Theta = (\theta-\theta_r)/(\theta_s-\theta_r)$ and $m=1-(1/n)$

α: shape parameter (cm^{-1})
n,l: shape parameters (-)
θ_r: residual water content (cm^3/cm^3)
θ_s: saturated water content (cm^3/cm^3)
K_s: saturated hydraulic conductivity (cm/hr)

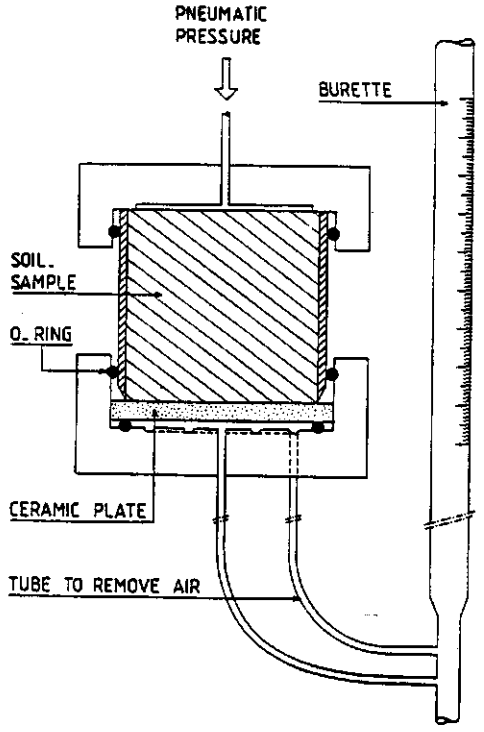

Fig. 11: Cross-section of pressure cell used in multi-step outflow method

2.6 EVAPORATION

Evaporation from bare soil was measured by using clear PVC micro-lysimeters with an inner diameter of 8.1 cm and a length of 12 or 17 cm. The cylinders were carefully pushed into the soil by hand. After lifting the soil-filled cylinder from the soil, the sample was pushed up inside the cylinder, so that the surface of the sample coincided with the top of the cylinder. The bottom was sealed to prevent water movement between the underlying soil and the sample. After weighing the micro-lysimeter, it was placed back in a preformed hole at a location comparable with the spot where the samples were taken. Every day, the micro-lysimeter was removed, weighed and replaced. Total evaporation between measurements was calculated from difference in mass.

The sealing of the bottom of the micro-lysimeter caused the soil in the micro-lysimeter to be wetter than the surrounding soil after precipitation. Therefore, the lysimeters were removed after a rainshower and new samples were taken. The experiment was started 2 to 3 days after a shower, thereby assuming that downward movement of water would not occur beyond that period.

Boast & Robertson (1991) described a laboratory experiment, where evaporation from micro-lysimeters of different lengths was measured for a wide range of initial soil water and evaporative conditions. It was shown that short lysimeters deviated from true evaporation rates sooner than longer ones. Moreover, the period during which measurements were correct was shorter for periods with high evaporative demand and wet initial conditions.

If upward movement of water occured, the evaporation measured by the micro-lysimeter

does not represent the evaporation of the surrounding soil. In order to correct for this a lysimeter of 12 cm and of 17 cm was installed with a mutual distance of ± 0.5 m at each spot in the field. It was assumed that until the evaporative loss of mass of the 2 micro-lysimeters differed, both cylinders represented the behaviour of the surrounding soil.

After the final experiment the moisture profile of several micro-lysimeters was measured in the laboratory. The samples were cut in slices, thickness and mass of each slice were measured and the moisture content was determined by oven-drying. In additional, moisture profiles in the field were determined directly near the hole after the micro-lysimeters were removed by TDR at depths of 4, 6, 8, 10, 12, 14 and 16 cm. A comparison of these profiles indicated whether the soil moisture regime in the micro-lysimeters was identical to the surrounding soil.

2.7 SOIL TEMPERATURE

At a bare soil location in the degraded bush (subsite d), a profile of TDR-probes with built-in temperature sensors was installed (Fig. 3 d). The probes were installed horizontally at depths of 2, 5, 10, 15 (no temperature sensor), 25, 30 (no temperature sensor) and 50 cm.
In general moisture content and soil temperature were measured every other day, using the FOM/mts instrument. The accuracy of the temperature measurement was 1°C. Temperature and moisture variations during a 24 hour period were measured on September 3 and October 7. At these days, measurements were taken every 30 minutes during daytime and every 1 or 2 hours in the evening and night. This included measurement of soil surface temperature using an infrared radiometer.

2.8 RAINFALL SIMULATION

A small rainfall simulator, originally developed by Kamphorst (1987), was used to collect information on the infiltration characteristics of the soil. The simulator discharges a rain shower at a standard intensity of 6 mm/min over a surface area of 0.0625 m^2. By measuring the amount of surface runoff, the infiltration rate can be calculated.
Fig. 12 shows a vertical cross section of the rainfall simulator with some adjustments to the original model (Brombacher & Eppink, in prep.). The gutter and frame (D and E) were placed on the test-plot; the sides of the surfaceframe were connected to the soil by using clay to prevent water leakage. The support, the reservoir and the sprinkler (A, B and C) were placed on the frame, while adjusting the length of the legs for horizontal placement. Sprinkling started through opening of the aeration pipe which was placed in the correct position to adjust the intensity of the rainshower to the required standard of 6 mm/min.
At several bare soil test-plots in the selected catchment, simulation measurements were made. The runoff-volume was collected after start of the experiment at every 30 seconds interval. Runoff-volume was measured immediately at the conclusion of the experiment. The duration of the rain shower varied between 4 and 6 minutes between spots and depended on the volume of water available in the reservoir. The slope of each test plot was determined by measuring the difference in length of the adjustable legs.

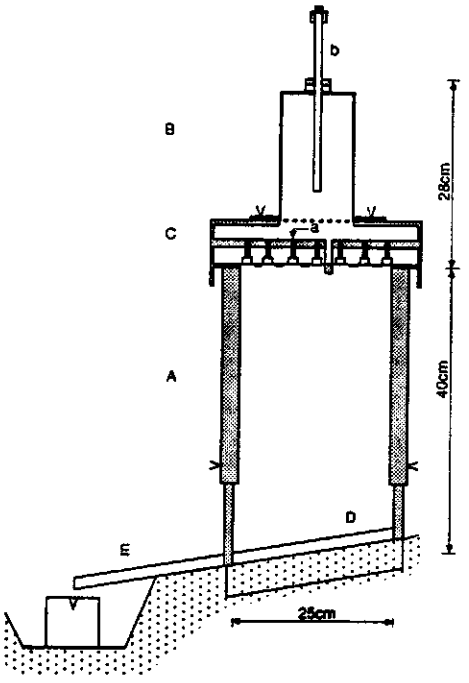

Fig. 12: The small rainfall simulator

2.9 SURFACE SOIL MOISTURE

Additional TDR-measurements of moisture content in the upper soil layer (0-10 cm depth) were taken on several days as supporting ground truth sampling for remote sensing (micro-wave) observations. Measurements were made in gridpatterns or in transects at all subsites (except the tiger-bush, subsite c) and at a sparcely covered millet field. The exact layout of the measurements is given in Fig. 13 a-f.

Moisture contents were measured through insertion of the 10 cm TDR-probe horizontally at 2, 5 and 10 cm depth and vertically. In general the mean value of horizontal measurements represented a single vertical measurement over the 10 cm depth adequatly.

2.10 GENERAL DOCUMENTATION

A general description of the subsites fallow bush (a), cleared grassland (a'), millet (b) and degraded bush (d) and of each (standard)plot, including vegetation, micro-relief and crust type, is given in appendix I. In addition to these descriptions each plot was photographed in the end of August. For several plots, a second photograph was taken at the beginning of October to document changes in vegetation during the SOP. A lay-out of each standard plot, with the position of TDR-probes and tensiometers, is given in Fig. 14 a-c.

Lay-outs of micro-lysimeters are given in appendix VI. For each of these locations, a photograph is available.

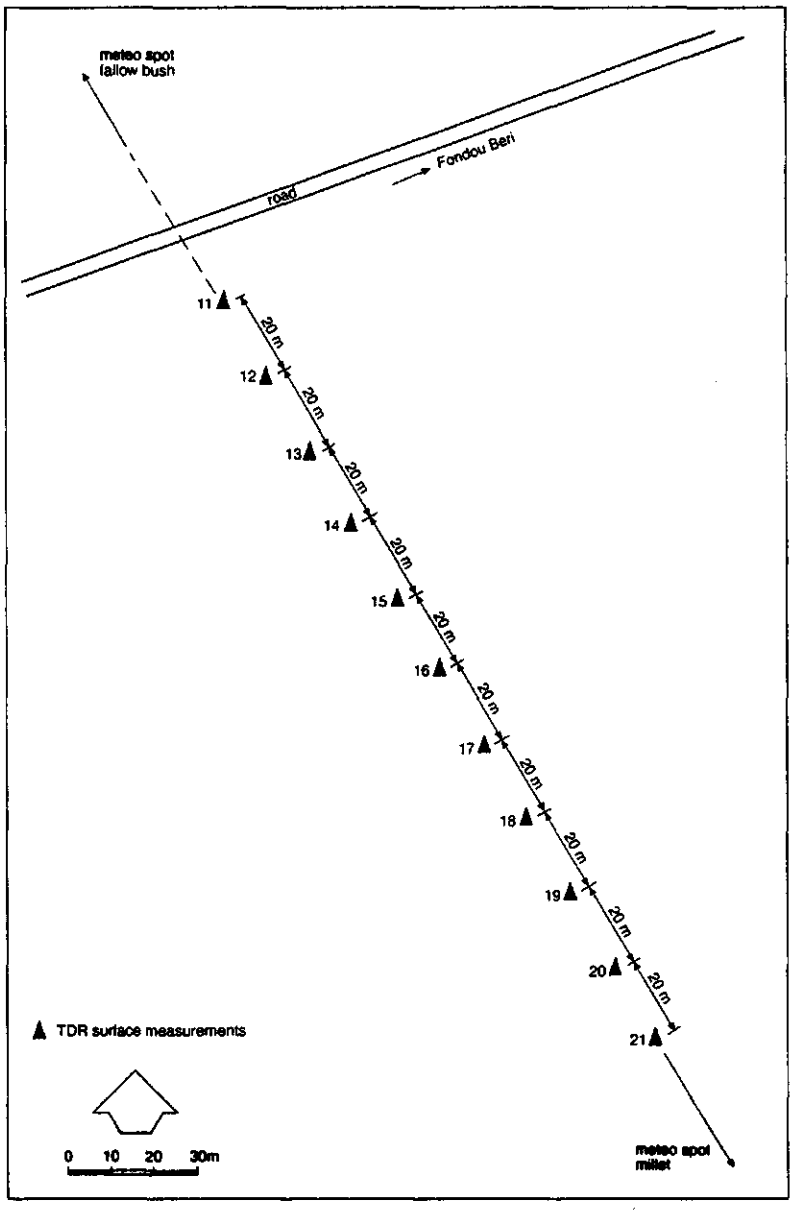

Fig. 13a: sparcely covered millet field August 23

Fig. 13: Lay-out of surfacial moisture content measurements at several locations

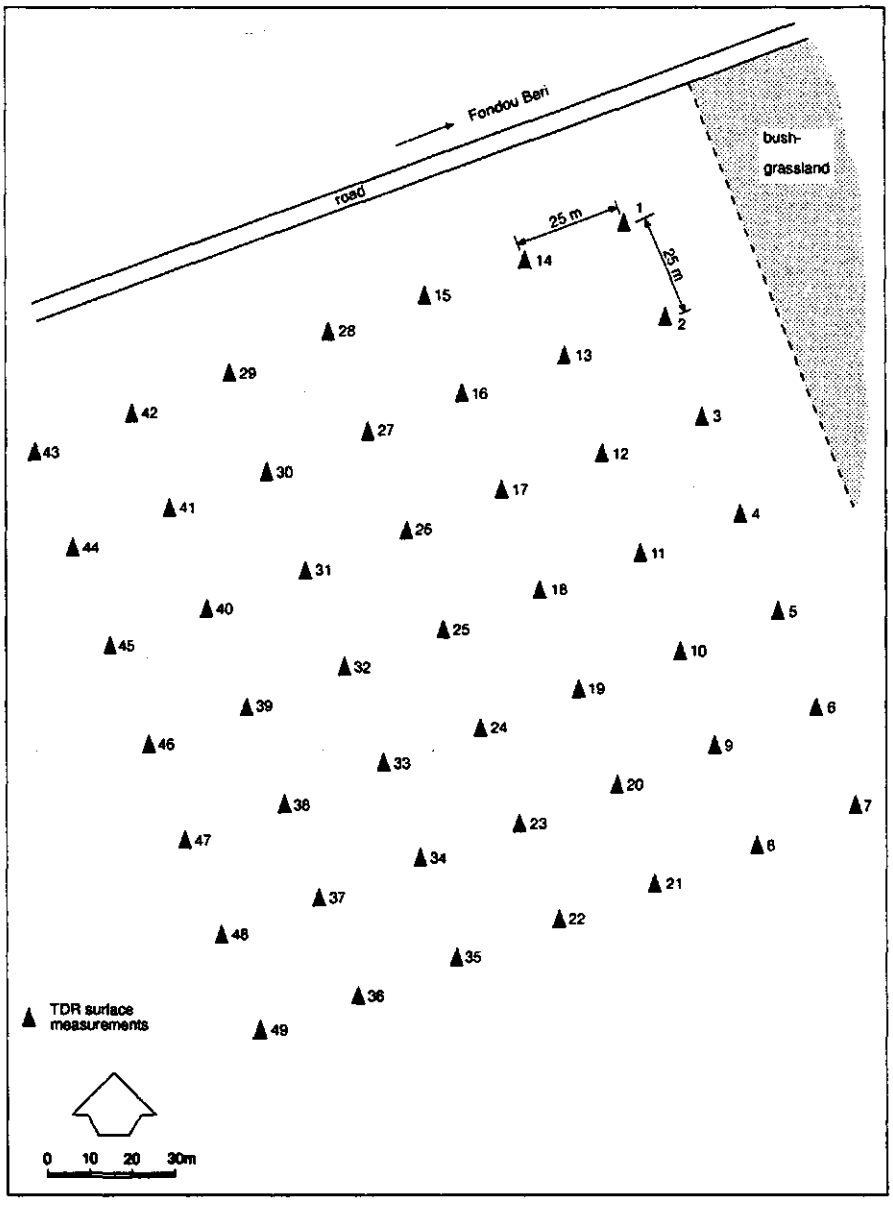

Fig. 13b: sparcely covered millet field August 25

Fig. 13: Lay-out of surfacial moisture content measurements at several locations

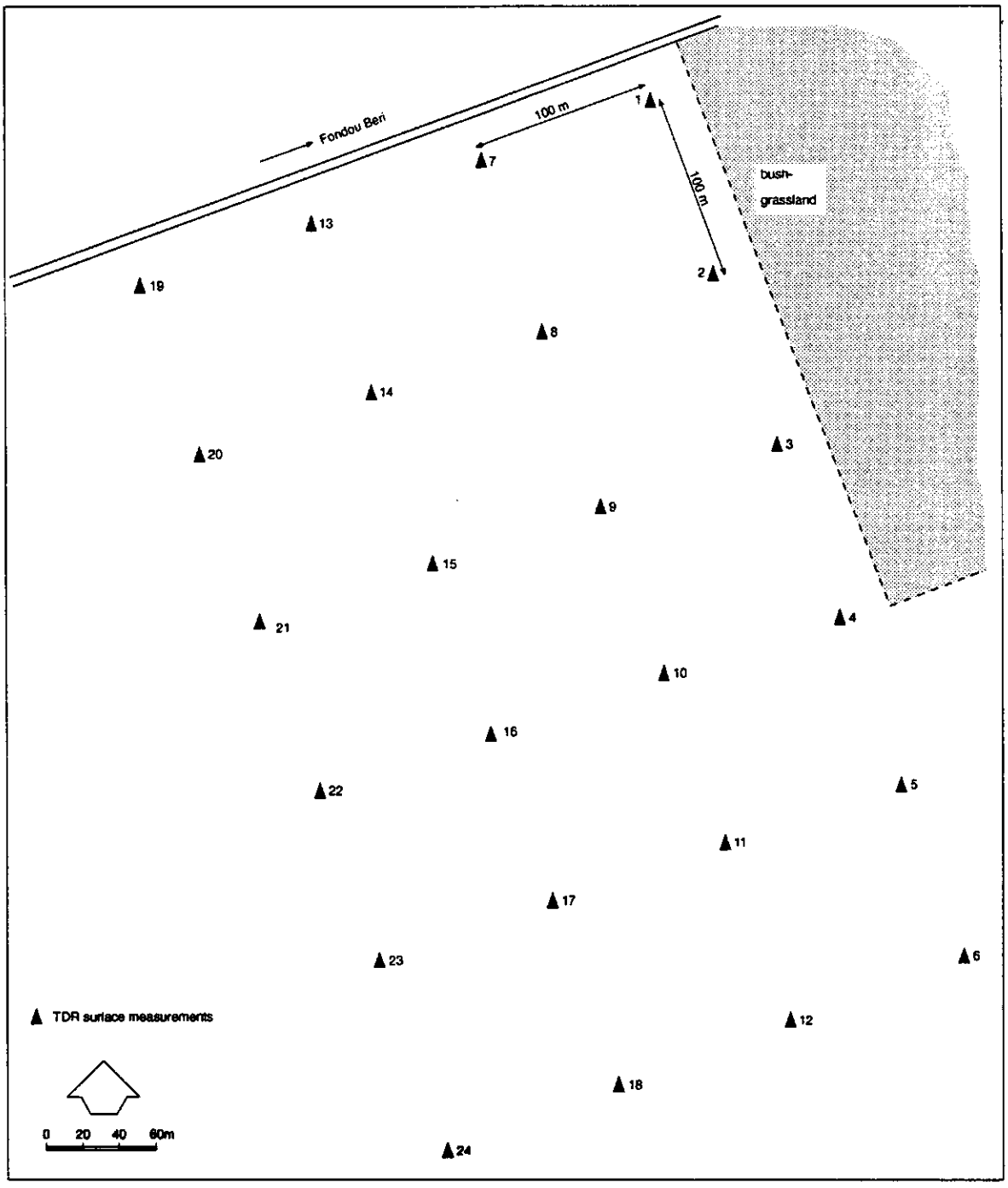

Fig. 13c: sparcely covered millet field August 26, September 9 and September 12

Fig. 13: Lay-out of surfacial moisture content measurements at several locations

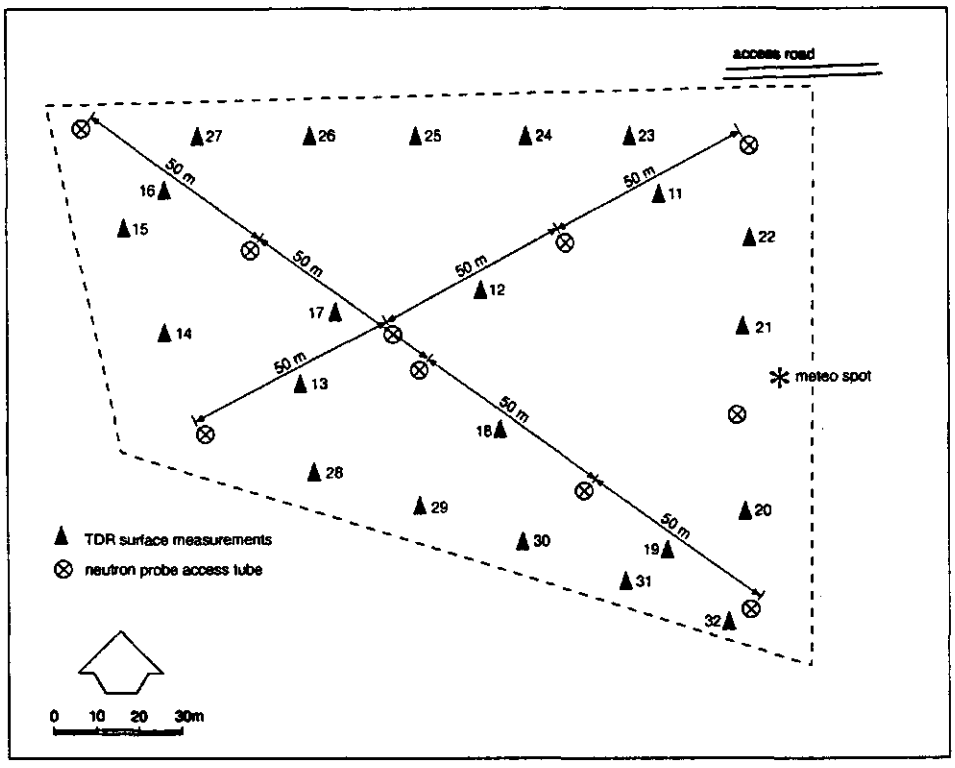

Fig. 13d: subsite millet August 25

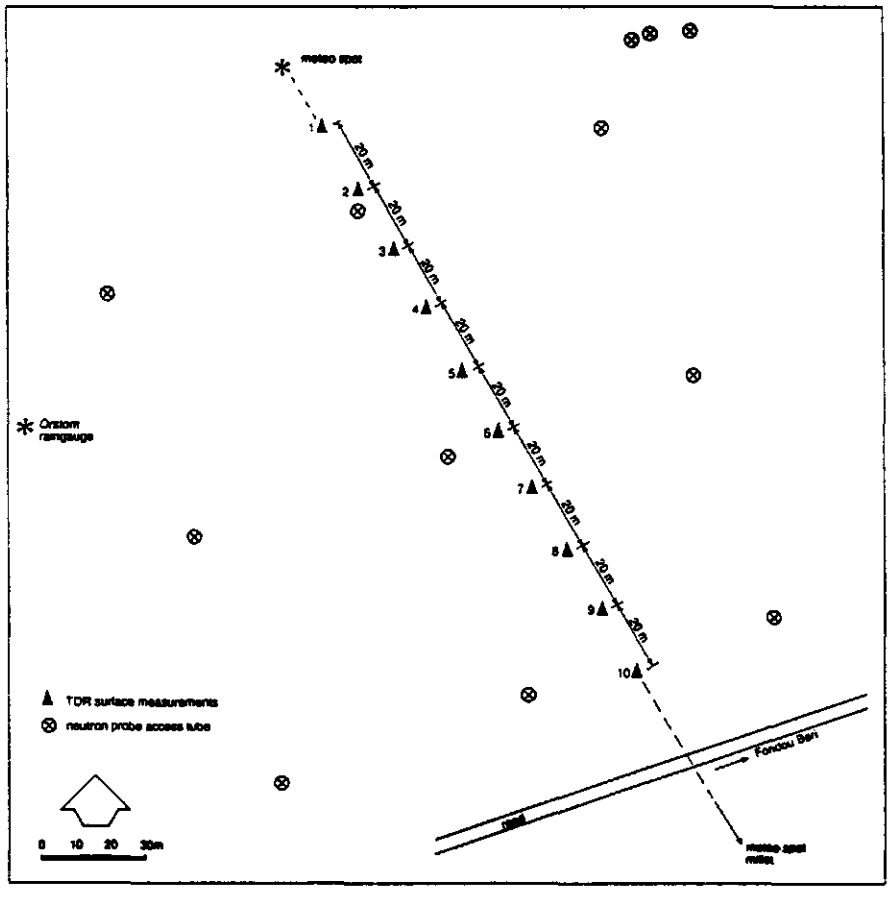

Fig. 13e: subsite fallow bush August 23

Fig. 13: Lay-out of surfacial moisture content measurements at several locations

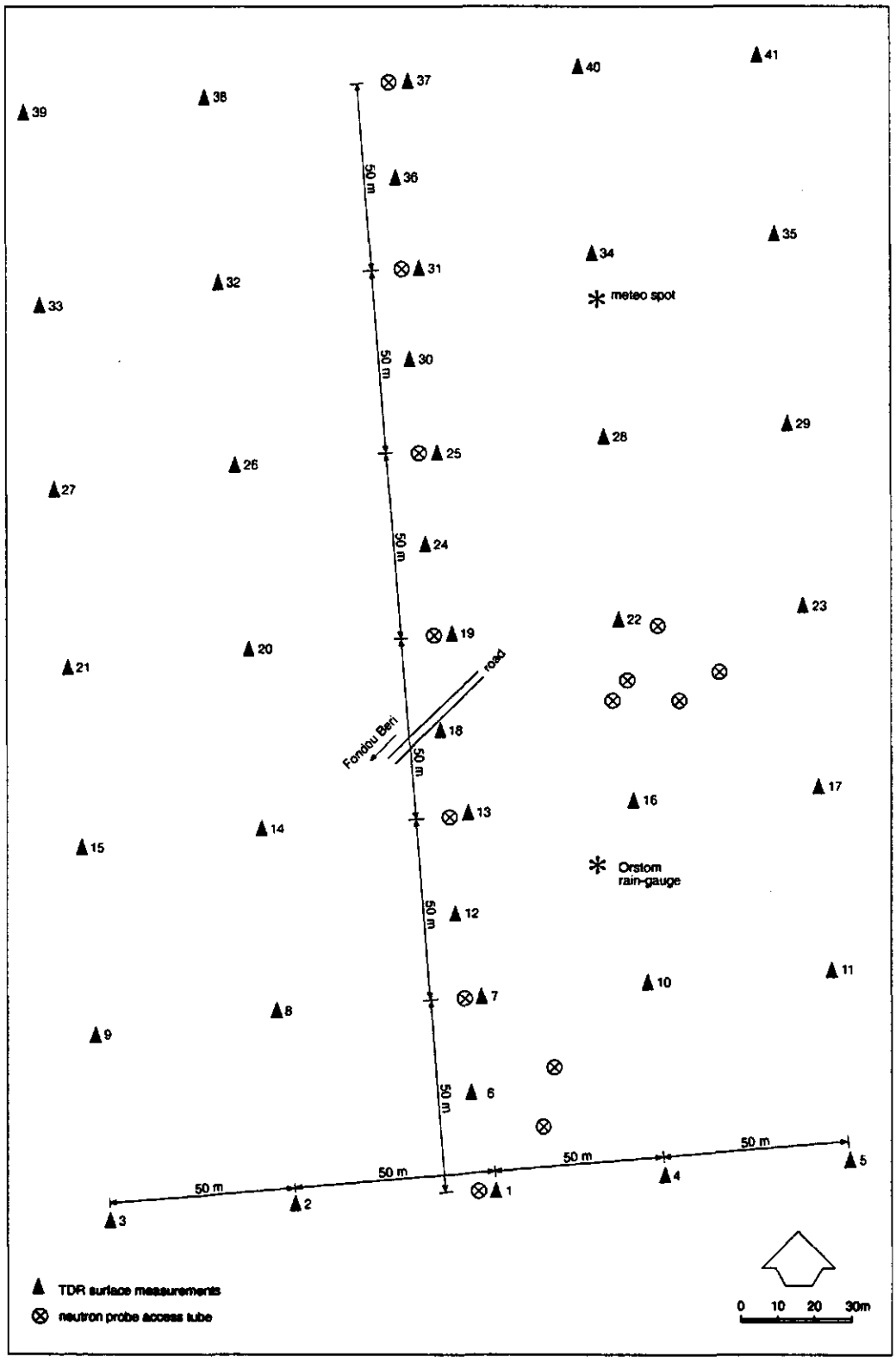

Fig. 13f: subsite degraded bush August 25, September 2 and September 12

Fig. 13: Lay-out of surfacial moisture content measurements at several locations

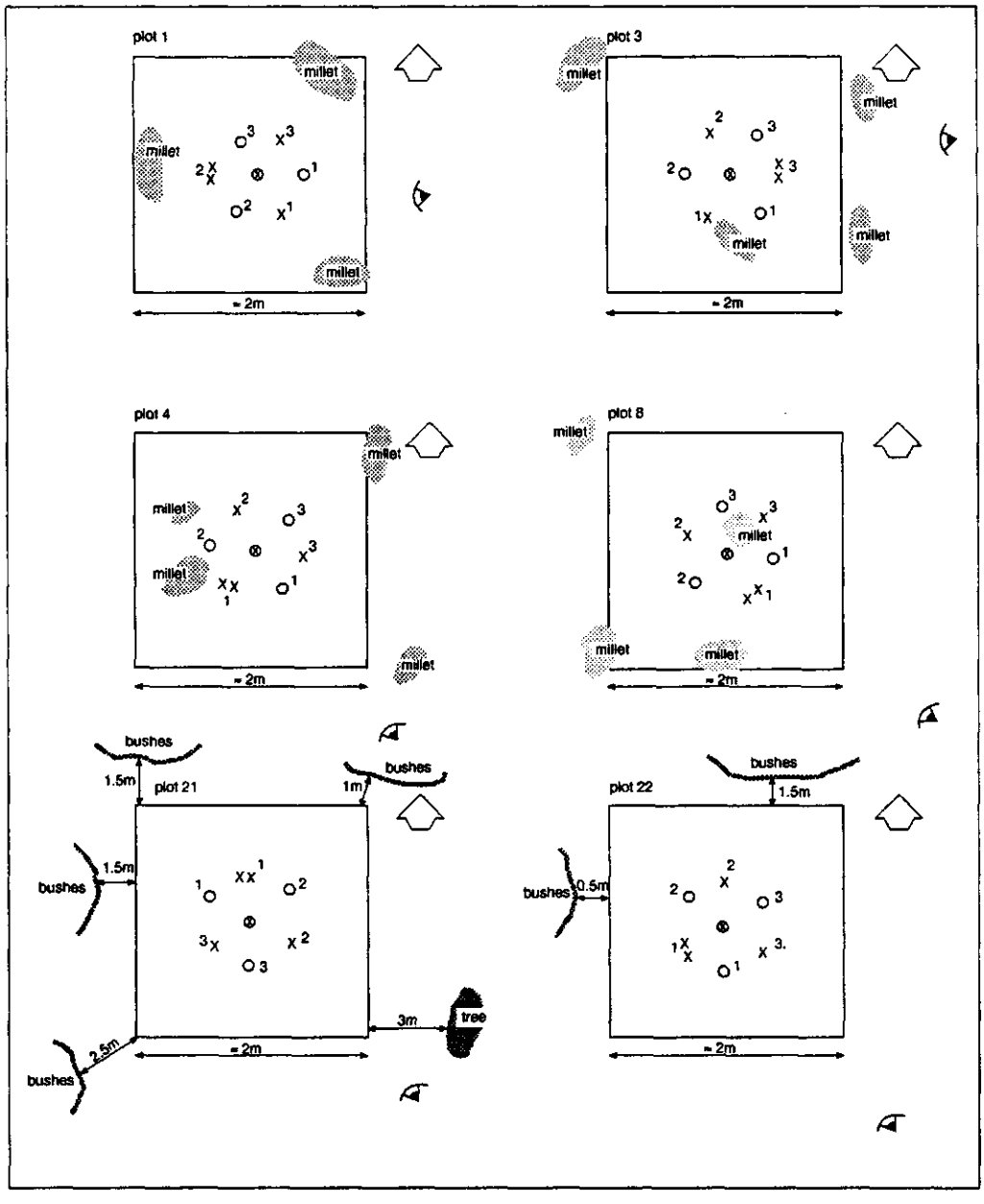

Fig. 14a: standard plots at subsites millet and fallow bush, nrs 1, 3, 4, 8, 21 and 22

Fig. 14: Surroundings of the standard plots

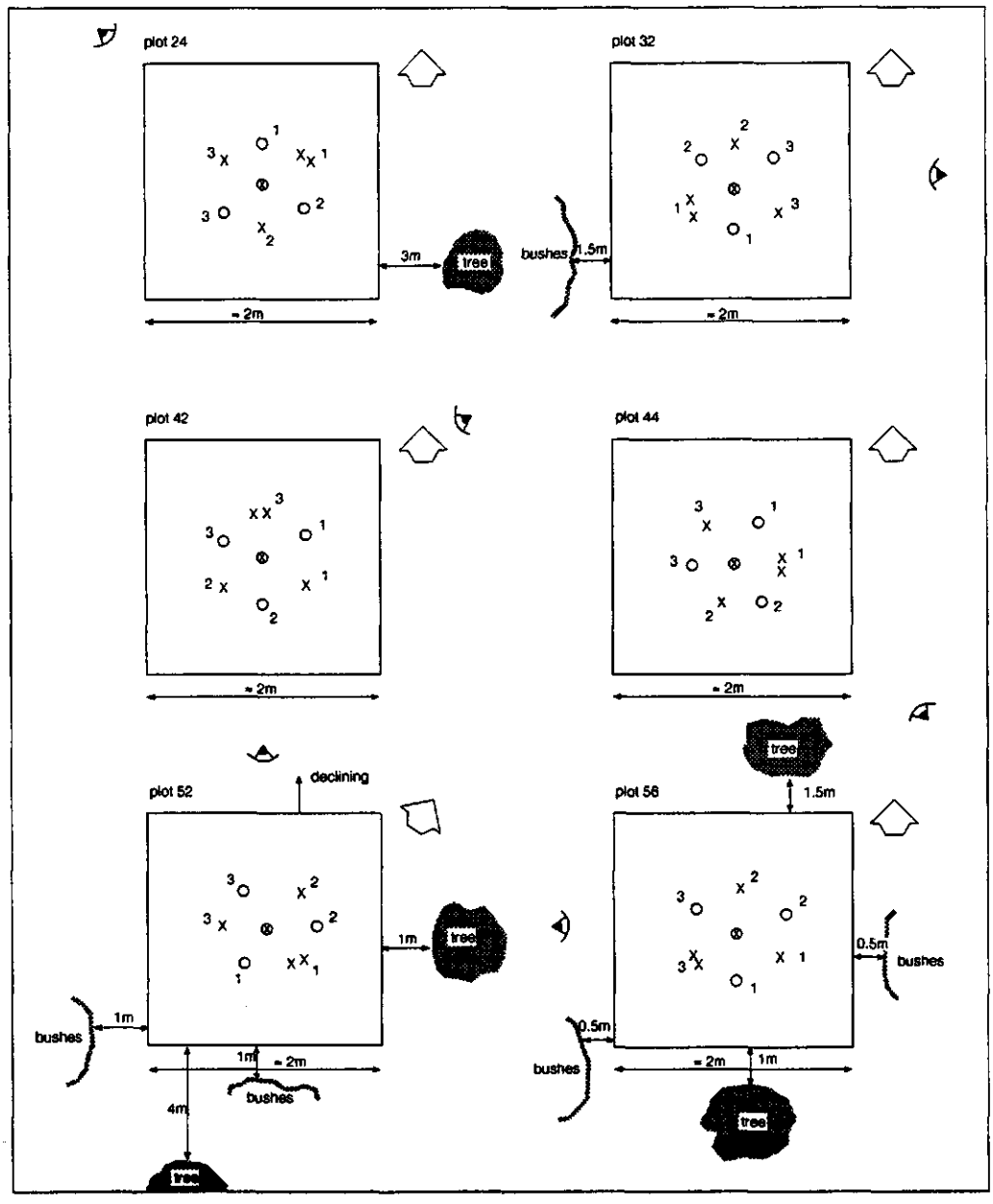

Fig. 14b: standard plots at subsites fallow bush, grassland and degraded bush, nrs. 24, 32, 42, 44, 52 and 56

Fig. 14: Surroundings of the standard plots

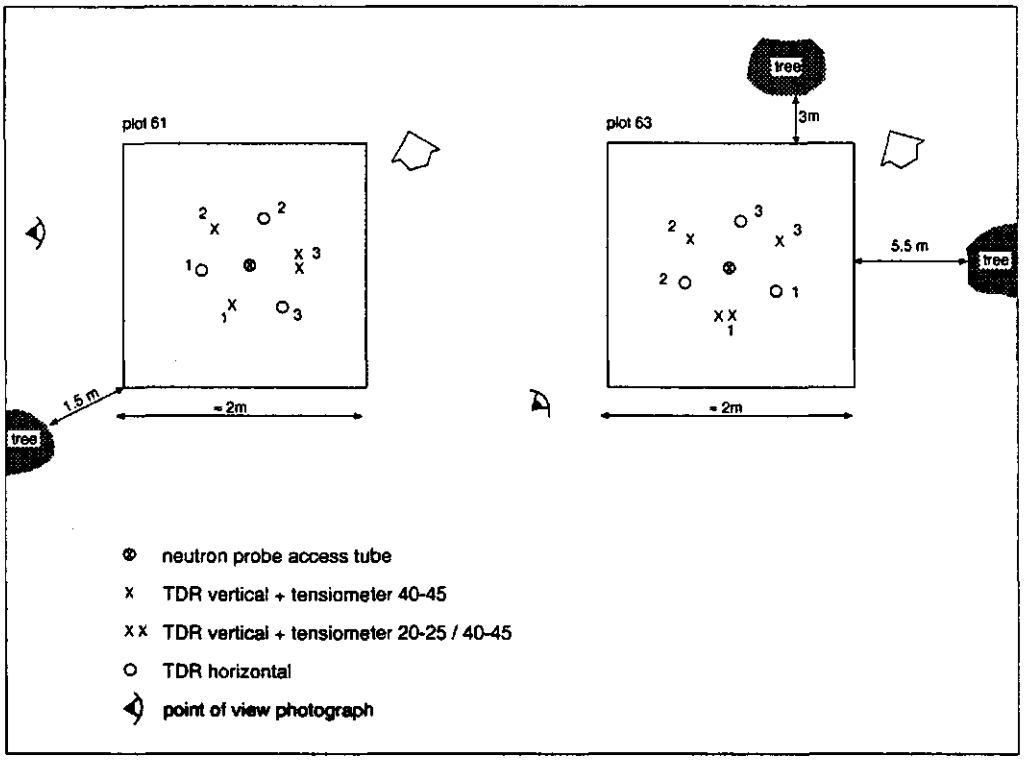

Fig. 14c: standard plots at subsite degraded bush, nrs. 61 and 63

Fig. 14: Surroundings of the standard plots

3 BRIEF DESCRIPTION OF DATASETS

3.1 SOIL MOISTURE

Results of neutron probe measurements have been stored in the files COUNTRAT.DAT (count ratio), STANDCTS.DAT (standard counts), and CTSTHETA.DAT (calibrated moisture content). For many locations measurements were not made exactly at the denoted depths. Corrections for depth are given in appendix III. Results of TDR-measurements are stored in the files DIEL.DAT (measured dielectric constant), DIELCAL.DAT (calibrated dielectric constant) and TDRTHETA.DAT (calibrated moisture content).

Fig. 15 a-c show changes in soil moisture profile during the SOP at three standard plots. In several cases the neutron probe measurements at 15 cm depth cause a discontinuity of the moisture profiles using TDR-measurements at 5 and 10 cm depth. Possibly measured count rate was reduced due to the escape of fast neutrons to the atmosphere while using the calibration curve of the 25 and 45 cm depth. Correction factors have been developed experimentally to be used with the normal calibration. Greacen (1981) gave the following relationship for the correction factor C as a function of moisture content θ:

$$\log(C-1) = -0.8453 \log\theta - 1.8446 \quad (50)$$

$$\log(C-1) = -0.5416 \log\theta - 1.9769 \quad (51)$$

for the 15 and 20 cm depth, respectively. Values of C have to be determined by optimization of $n_c = C \cdot n_m$, combined with the calibration curves given in 2.1.1 (n_c and n_m are corrected and measured count rates respectively). Final values of the correction factor have not been determined, yet.

3.2 SOIL WATER SUCTION

Direct read-outs of the pressure transducer system have to be corrected for the height of the water column inside the tensiometer (+ 40 cm) to calculate the soil water suction at the level of the ceramic cup. Corrected data are given in the file TENSIO.DAT.

Combining measured suction with TDR-measurements at a similar depth and location (see Fig. 2) results i an in situ retention curve. Preliminary results are given in Fig. 16 a-l.

3.3 CATCHMENT

Not all the runoff registrations were successful due to side-flow along the flume and problems with the registration system. A waterlevel decline in the flume was not recorded accurately by the system. Only after a certain fall in waterlevel the actual head was recorded, thereby resulting in a discontinuous registered decline of head. After recalibration of the registration system in the laboratory a final set of discharge data of 6 events was selected. The data are stored for each event separately in the files RUNdate.DAT, including corrected values of head, calculated runoff and 5 minute

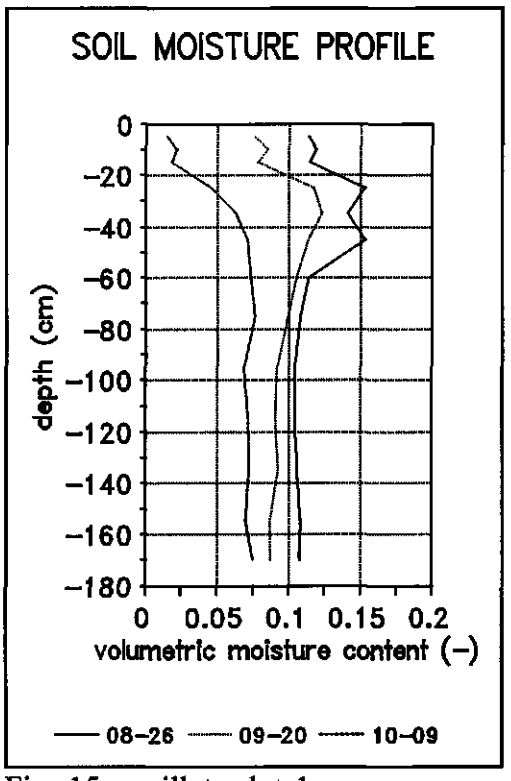

Fig. 15a: millet, plot 1

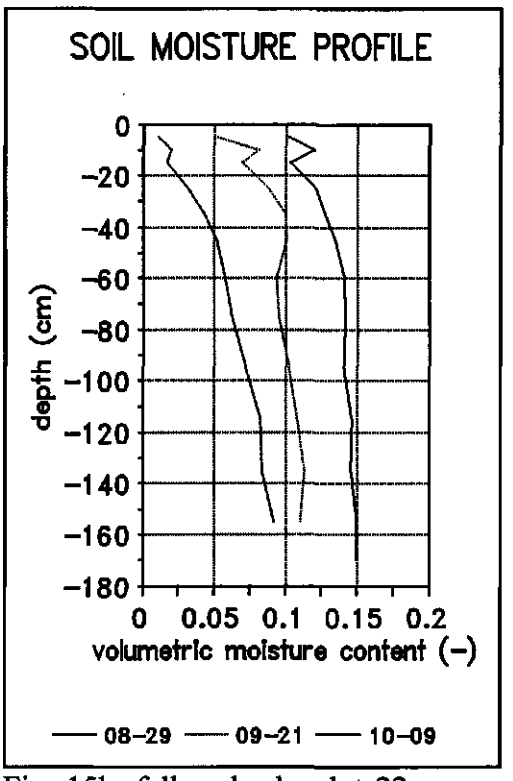

Fig. 15b: fallow bush, plot 22

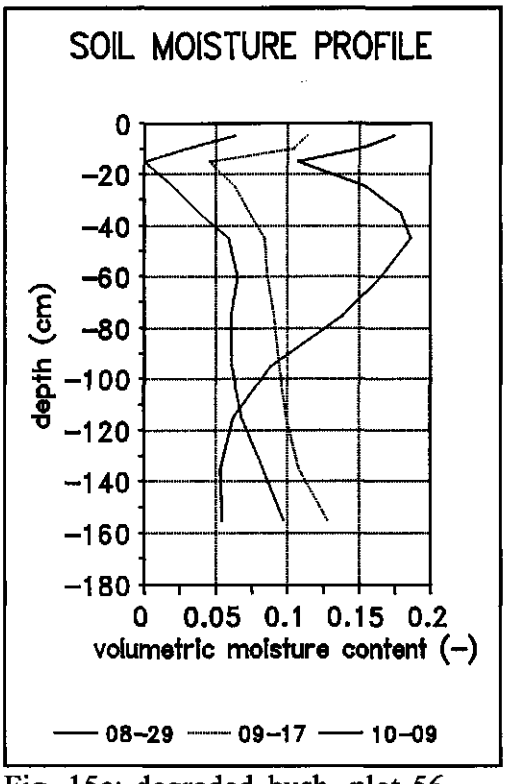

Fig. 15c: degraded bush, plot 56

Fig. 15: Soil moisture profiles of three plots showing results of three observation dates

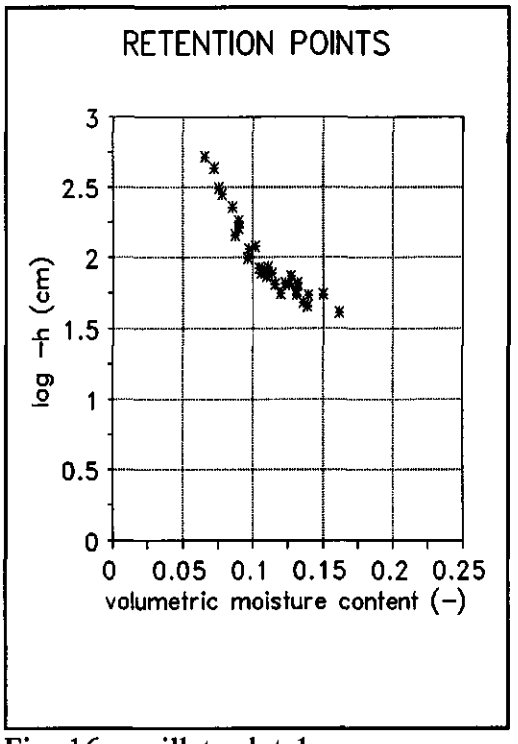

Fig. 16a: millet, plot 1
depth 25 cm

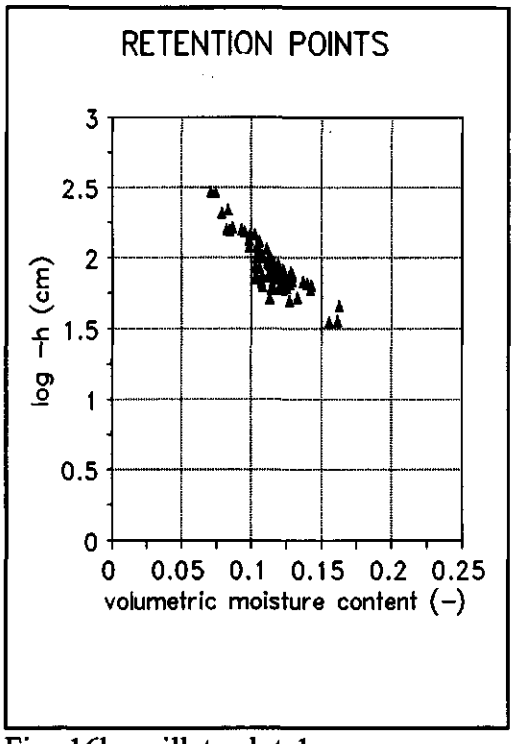

Fig. 16b: millet, plot 1
depth 45 cm

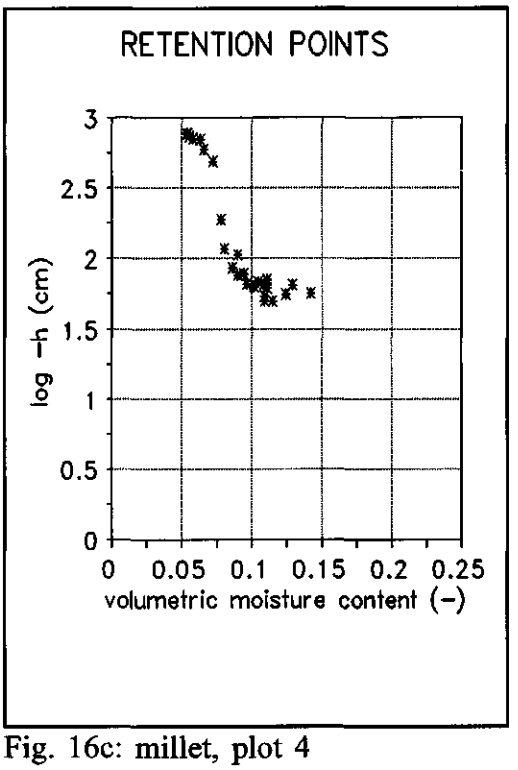

Fig. 16c: millet, plot 4
depth 25 cm

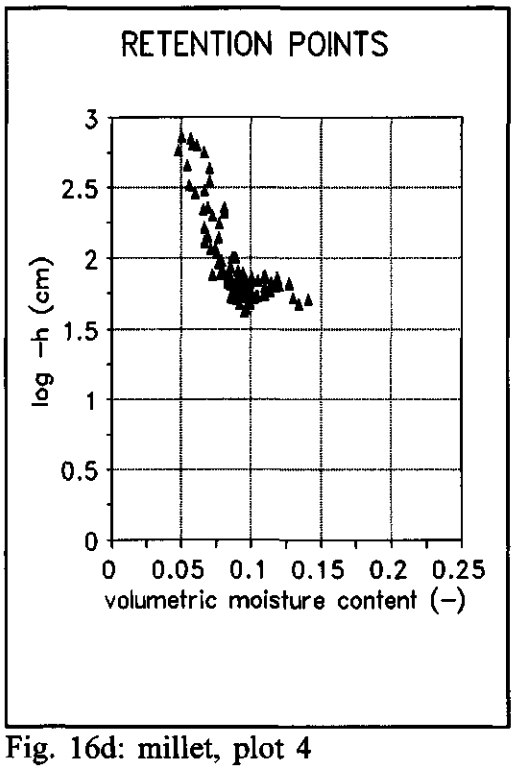

Fig. 16d: millet, plot 4
depth 45 cm

Fig. 16: Retention data of in situ measured soil moisture by TDR and soil suction by tensiometry

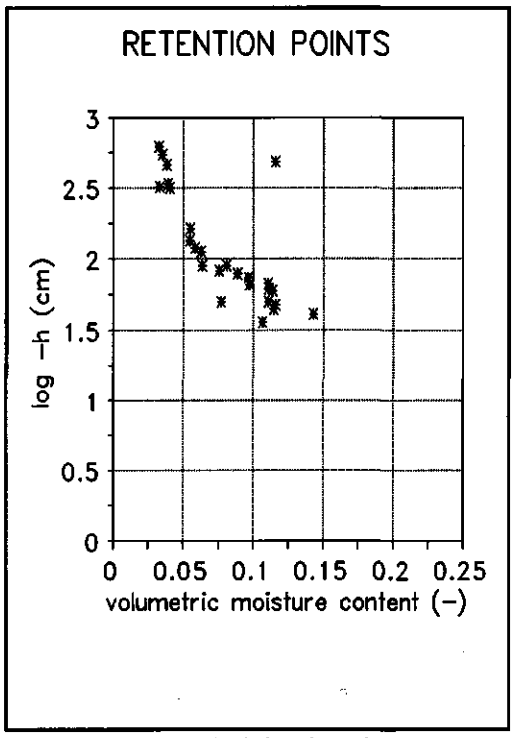

Fig. 16i: degraded bush, plot 56 depth 25 cm

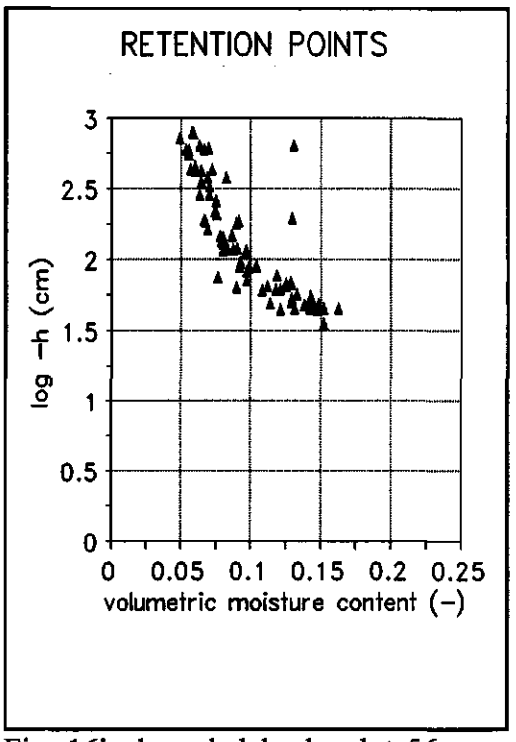

Fig. 16j: degraded bush, plot 56 depth 45 cm

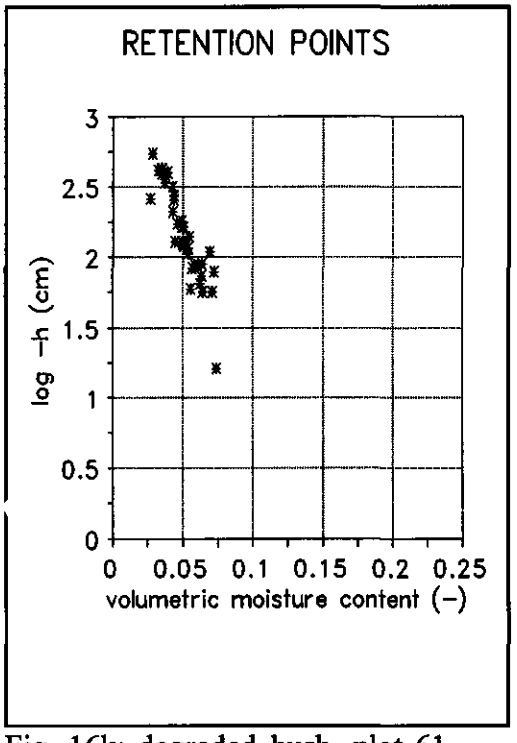

Fig. 16k: degraded bush, plot 61 depth 25 cm

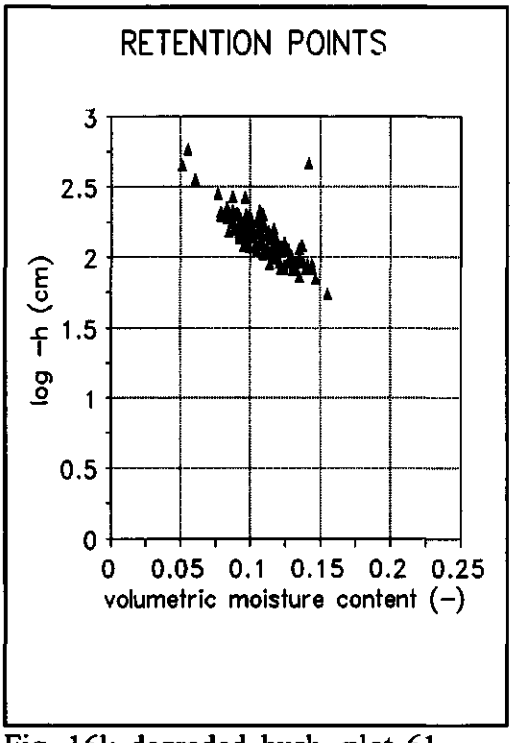

Fig. 16l: degraded bush, plot 61 depth 45 cm

Fig. 16: Retention data of in situ measured soil moisture by TDR and soil suction by tensiometry

values of precipitation.
An important point of consideration is how far the contributing area to total runoff has varied. From the topographic survey it became clear that some parts of the catchment boundary were contributing depending on the rainfall-intensity. Also, at one point 'strange' water was flowing in from an adjacent catchment during a high rainfall intensity event.
A first calculation of runoff was made assuming the complete area contributed to the runoff. Results are shown in Fig. 17 a-f and Table 6.

Table 6: Selected rainfall events at micro-catchment, degraded bush

date	precipitation	surface runoff
Aug 8 1992	14.5 mm	0.6 mm
Aug 21 1992	44.7 mm *	16.8 mm
Aug 28 1992	35.5 mm	26.5 mm
Aug 30 1992 (a)	17.5 mm **	8.1 mm
Aug 30 1992 (b)	19.1 mm	25.0 mm
Sept 10 1192	9.5 mm	0.3 mm

* 21:30-22:55 gmt
** 2:05-2:50 gmt

3.4 IN SITU HYDRAULIC CONDUCTIVITY

The raw data have been stored for each experiment separately in the files DISCdate.DAT. In the filename, date indicates the first day of an experiment. In these files, the waterlevel in the bubble-tower z_1 is given; the tension at the supply membrane equals z_2-z_1 (z_2 = 0.7 cm). Appendix IV gives an overview of all measurements. Additional photographs of each measuring location and detailed pictures of different crust types are available.

The methods to determine the hydraulic conductivity are generally based on Wooding's solution for three-dimensional flow from a circular source on a homogeneous soil. In case measurements are made on the surface, the condition of a homogeneous soil is not met due to the existence of a surface crust. Therefore the method described by Ankeny et al. (1991) or Reynolds & Elrick (1991) has to be adjusted to include the assumed vertical flow through the crust. Another possibility might be to approach the flow process by numerical simulation. This has not been worked out, yet. Also, the hydraulic properties of the soil samples have not been measured yet.
Some preliminary results are shown in Fig. 18 and 19. The influence of the crust on the infiltration rate is shown in Fig. 18 a-c. For measurements at the subsurface a homogeneous soil can be assumed and, ignoring the vertical flow through the upper 0.5 cm, the hydraulic conductivity can be calculated (Fig. 19 a-c).
Problems that occured in some cases during the measurements are summarized:

- The steady state flow rate increased after refilling the waterreservoir, while the waterlevel in the bubble-tower was kept constant. This indicates that the soil was disturbed by removing the disc permeameter.
- Steady state flow rates were constant over several pressure steps or even diminished with increasing supply pressure, yielding negative values for calculated hydraulic conductivities.

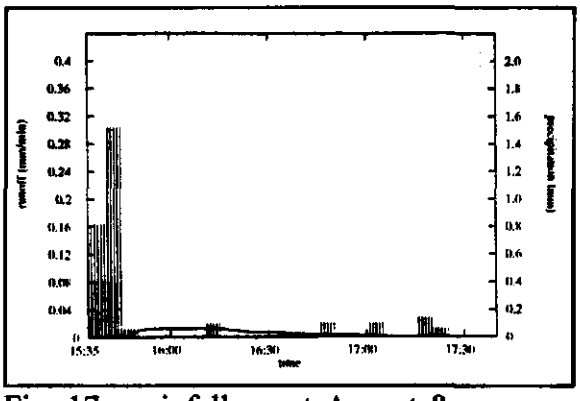

Fig. 17a: rainfall event August 8

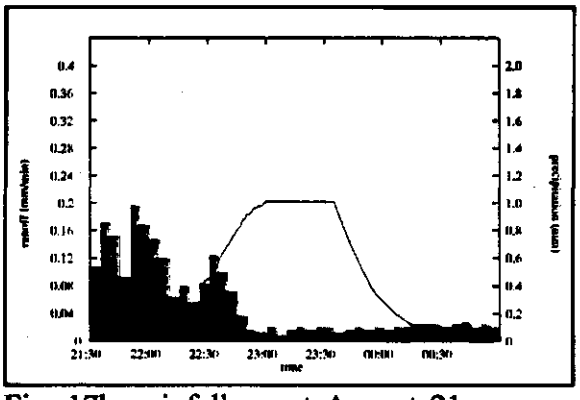

Fig. 17b: rainfall event August 21

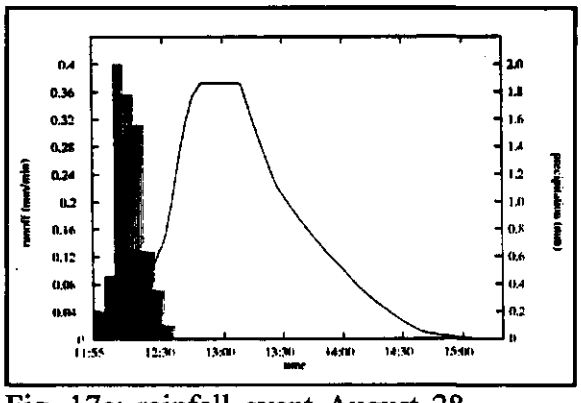

Fig. 17c: rainfall event August 28

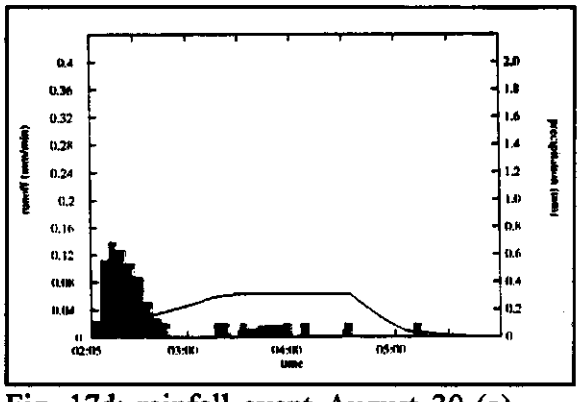

Fig. 17d: rainfall event August 30 (a)

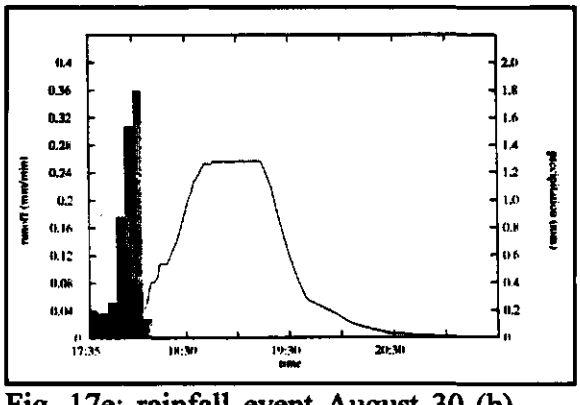

Fig. 17e: rainfall event August 30 (b)

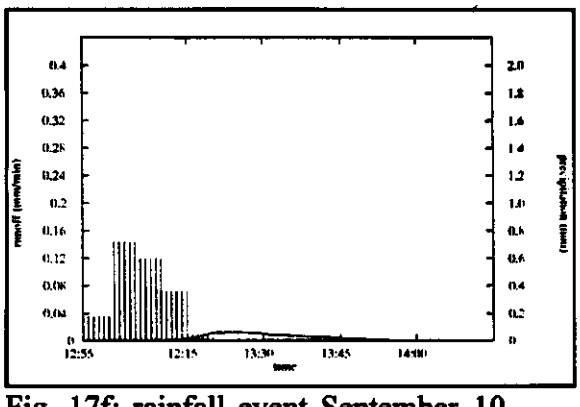

Fig. 17f: rainfall event September 10

Fig. 17: Selected runoff events at micro-catchment, subsite degraded bush

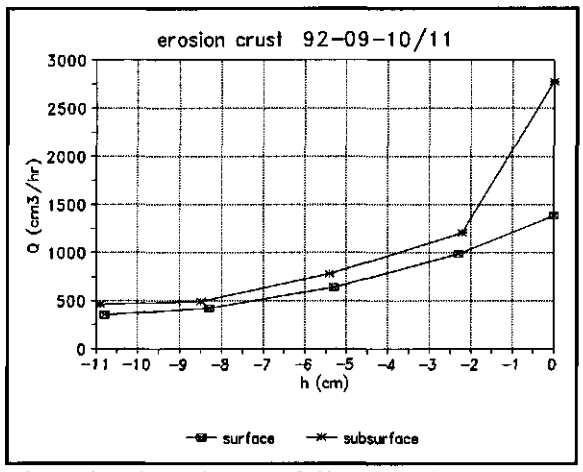

Fig. 18a: location at fallow bush

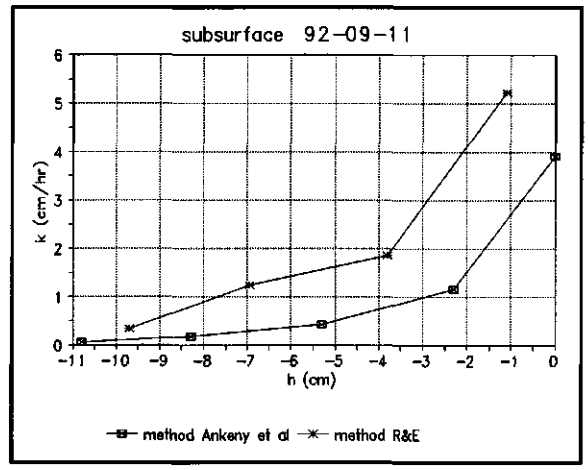

Fig. 19a: location at fallow bush

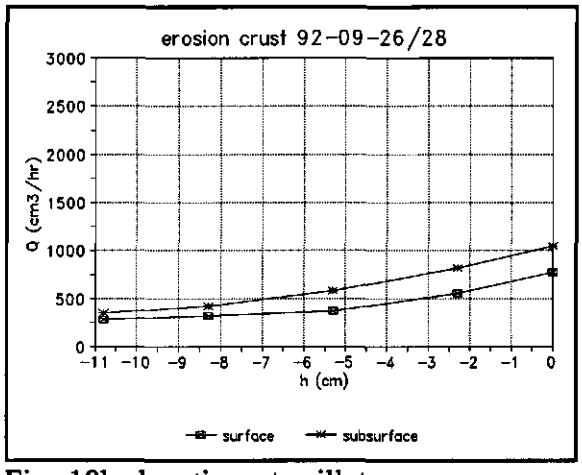

Fig. 18b: location at millet

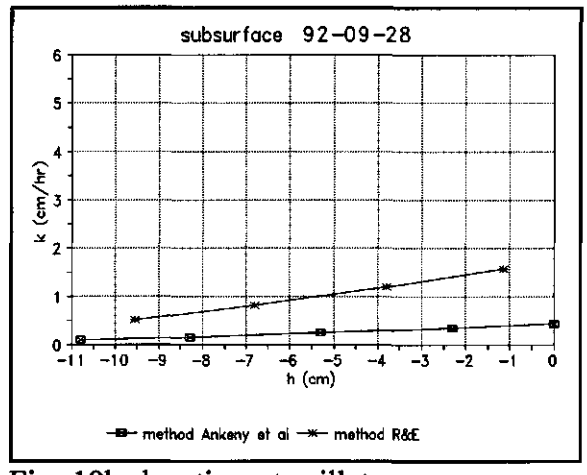

Fig. 19b: location at millet

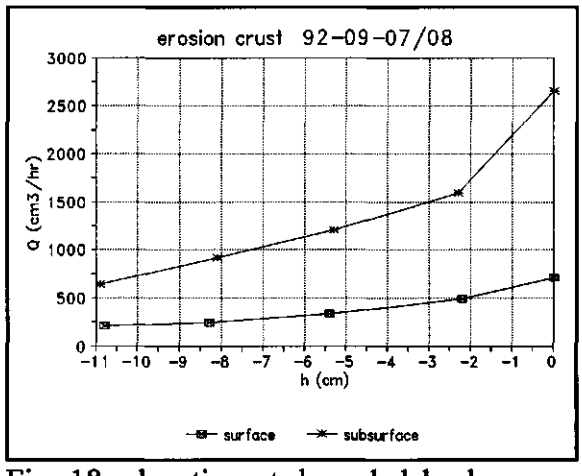

Fig. 18c: location at degraded bush

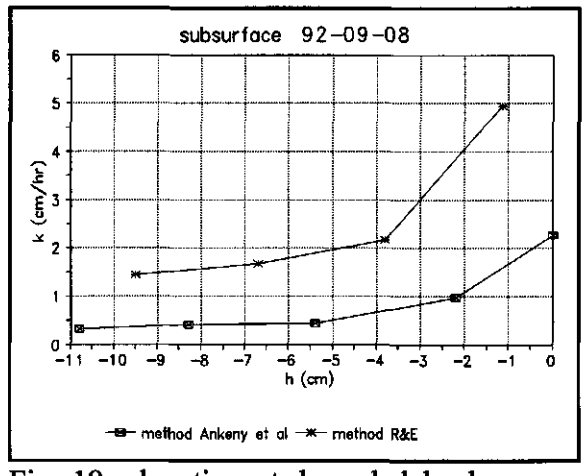

Fig. 19c: location at degraded bush

Fig. 18: The disc permeameter steady state flowrate for various suction heads

Fig. 19: Hydraulic conductivity of the subsurface, calculated by two different methods

3.5 SOIL HYDRAULIC PROPERTIES

At the subsites fallow bush, millet and degraded bush undisturbed soil samples were taken. In appendix V a review is given of all the collected samples. The soil hydraulic properties of these samples have not been determined yet.
Some additional samples were taken at the Northern Satellite site near the village of Danguey Gorou. The sample locations are depicted in Fig. 20.

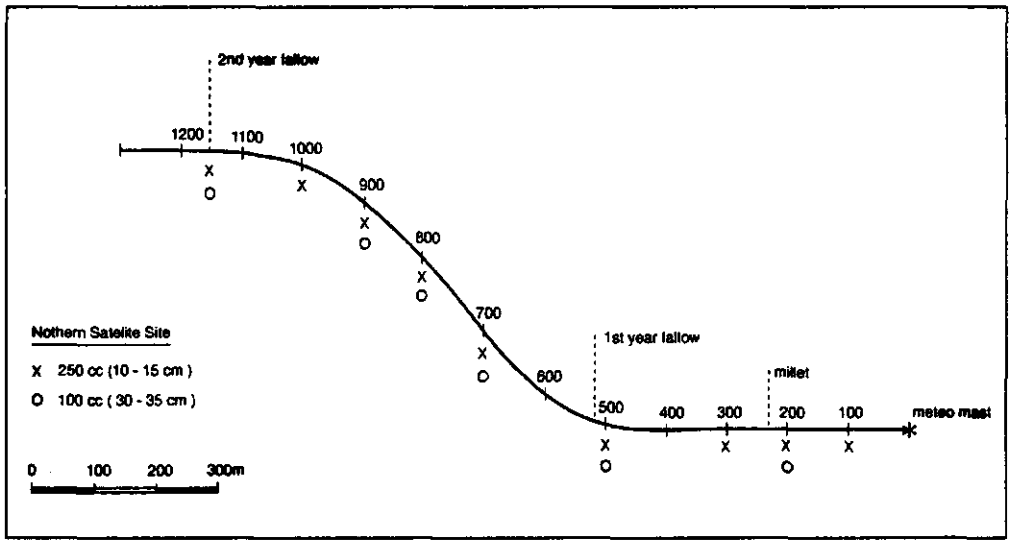

Fig. 20: Sample locations at the Northern Satelitte site

3.6 EVAPORATION

Evaporation of bare soil has been measured at several spots in the subsites fallow bush, grassland and degraded bush (appendix VI). At subsite b (millet) the upper soil, consisting of loose sand, was often blown on top of the micro-lysimeters, causing serious errors in measurements. For that reason these data have been excluded.
Results have been stored in the files MICROLYS.DAT and LYSPROF.DAT.
Fig. 21 a-f and 22 a-c show calculated evaporation and measured moisture profiles at the end of the experiment respectively. Data still have to be analyzed.

3.7 SOIL TEMPERATURE

Measured soil temperature and calibrated moisture content are stored in the file TEMPPROF.DAT. Temperature changes during a 24 hour period are shown in Fig. 23 a-b.

3.8 RAINFALL SIMULATION

At seven test-plots of different slope, varying between 2.5% and 17%, rainfall-runoff measurements were made. The infiltration rate was calculated for each experiment at 30 seconds intervals, using the rain shower intensity and runoff amounts. Results have been stored in the file RAINSIM.DAT and are shown in Fig. 24 a-g.

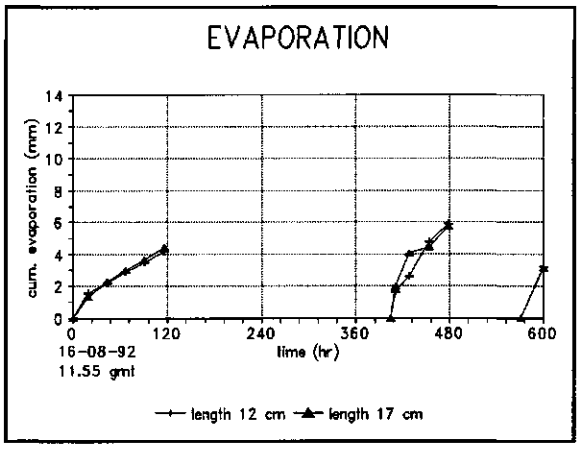

Fig. 21a: fallow bush, plot 21

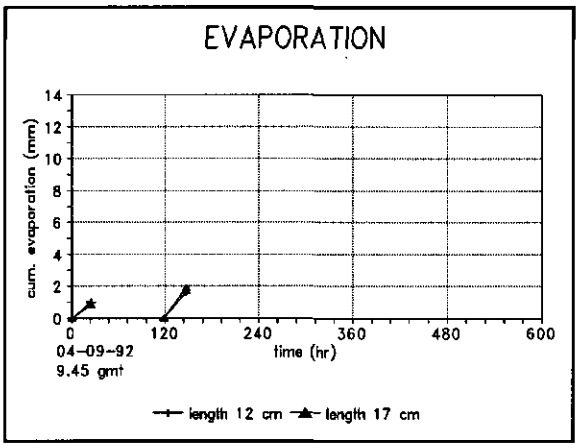

Fig. 21b: fallow bush, plot 22

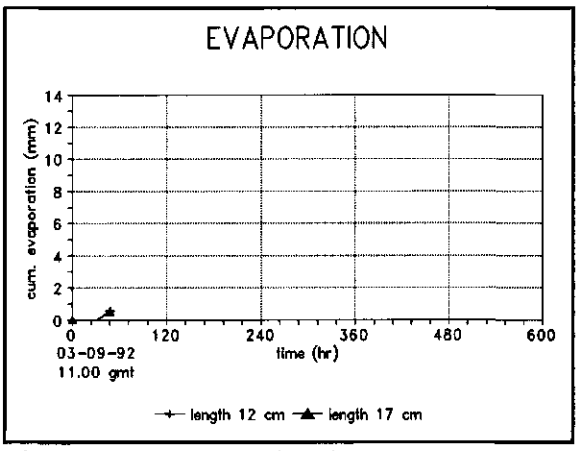

Fig. 21c: fallow bush, plot 25

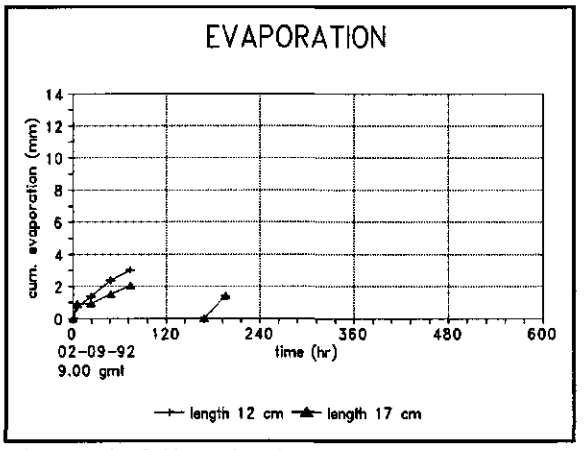

Fig. 21d: fallow bush, plot 28

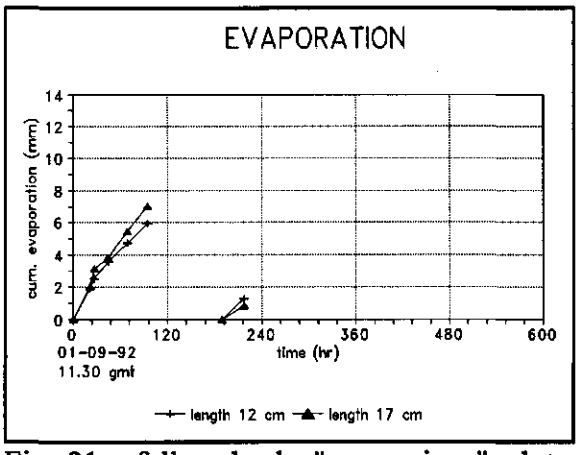

Fig. 21e: fallow bush, "comparison" plot

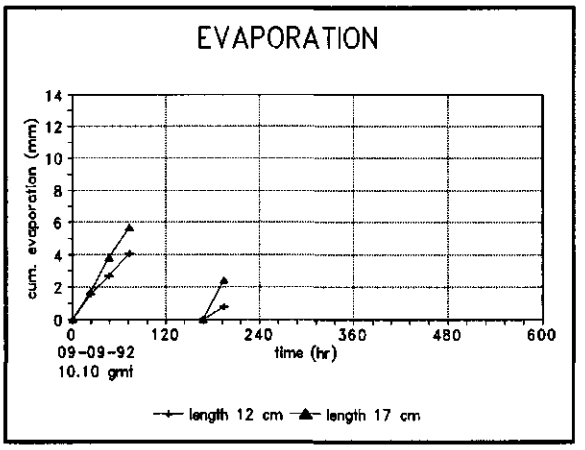

Fig. 21f: grassland, plot 42

Fig. 21: Evaporation results of the micro-lysimeter measurements

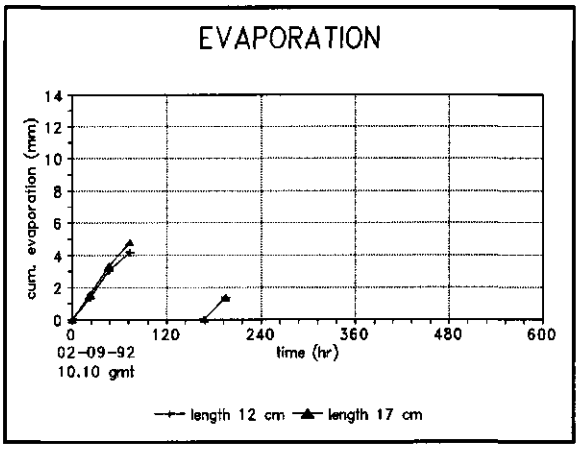

Fig. 21g: grassland, plot 44

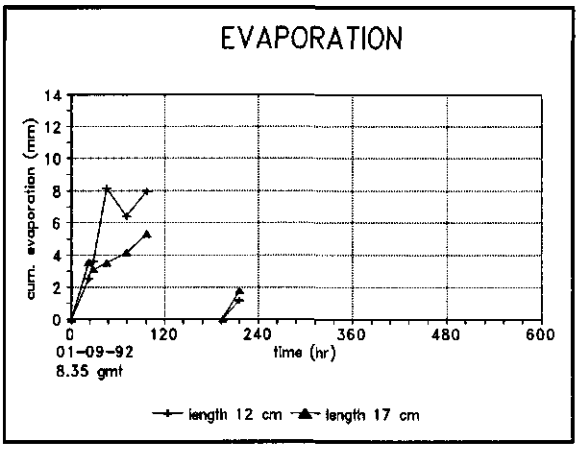

Fig. 21h: degraded bush, plot 52

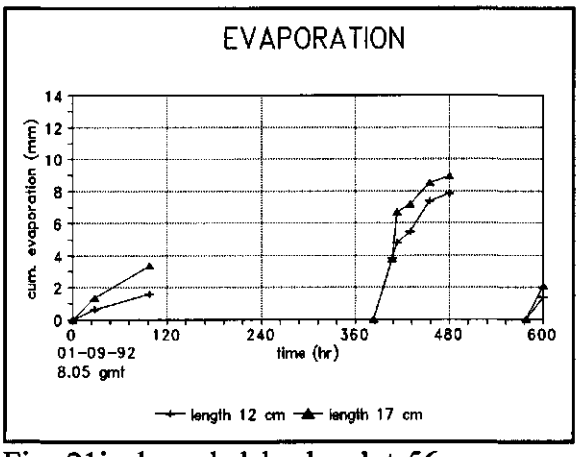

Fig. 21i: degraded bush, plot 56

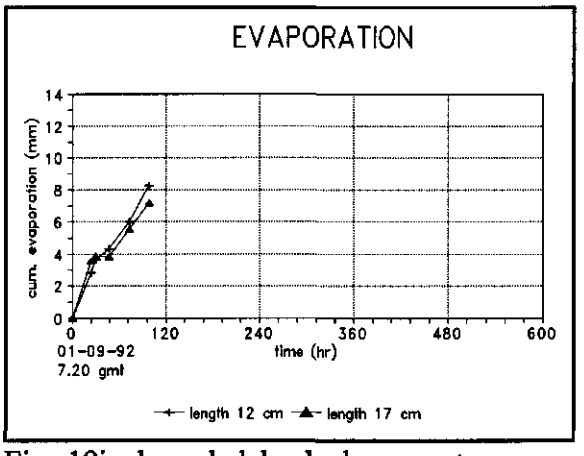

Fig. 19j: degraded bush, bare spot

Fig. 21: Evaporation results of the micro-lysimeter measurements

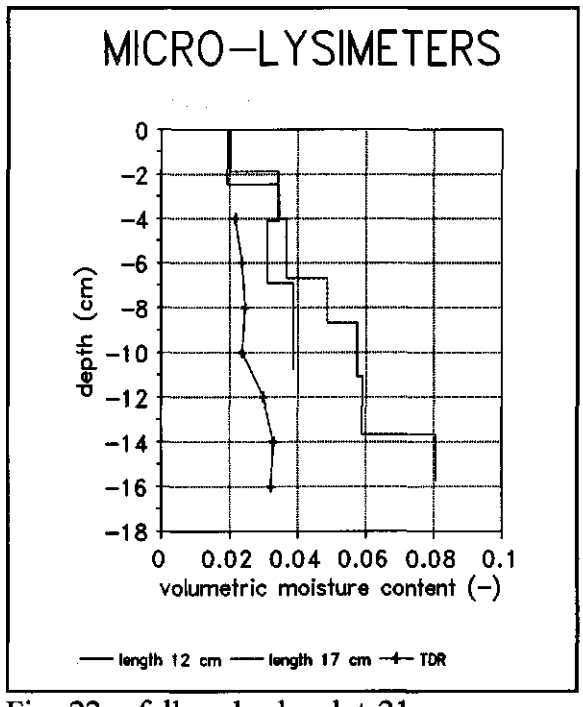

Fig. 22a: fallow bush, plot 21

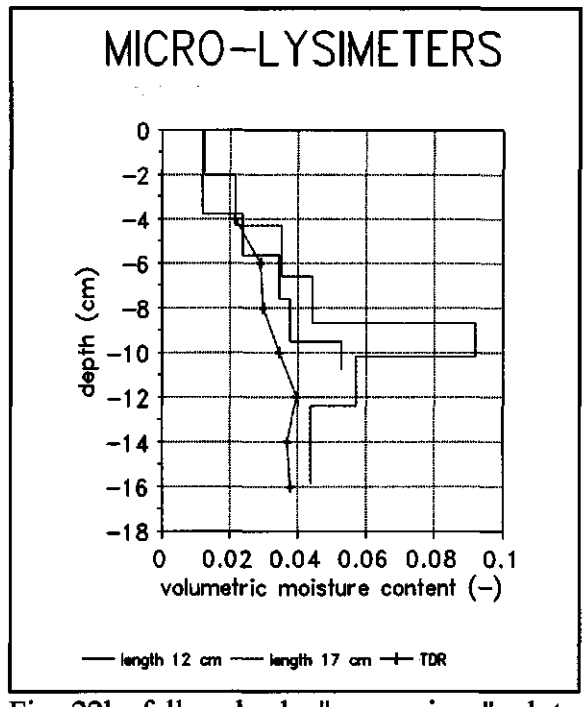

Fig. 22b: fallow bush, "comparison" plot

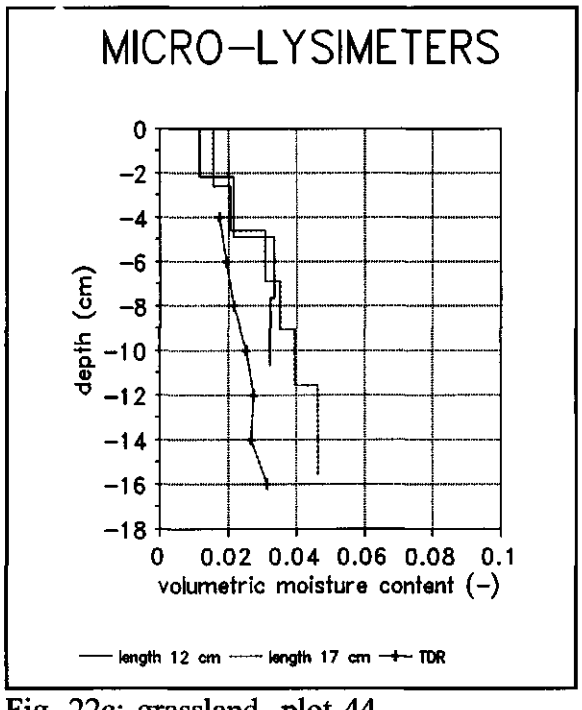

Fig. 22c: grassland, plot 44

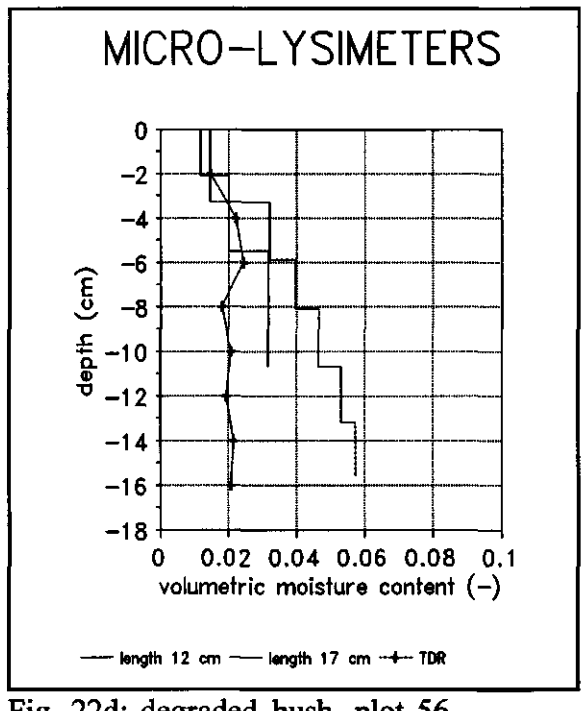

Fig. 22d: degraded bush, plot 56

Fig. 22: Moisture profiles of the micro-lysimeters and of a location in the very near surroundings

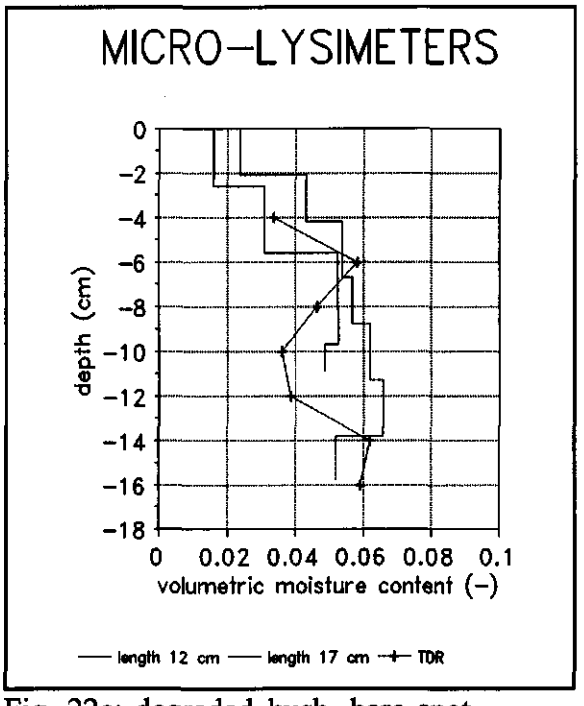

Fig. 22e: degraded bush, bare spot

Fig. 22: Moisture profiles of the micro-lysimeters and of a location in the very near surroundings

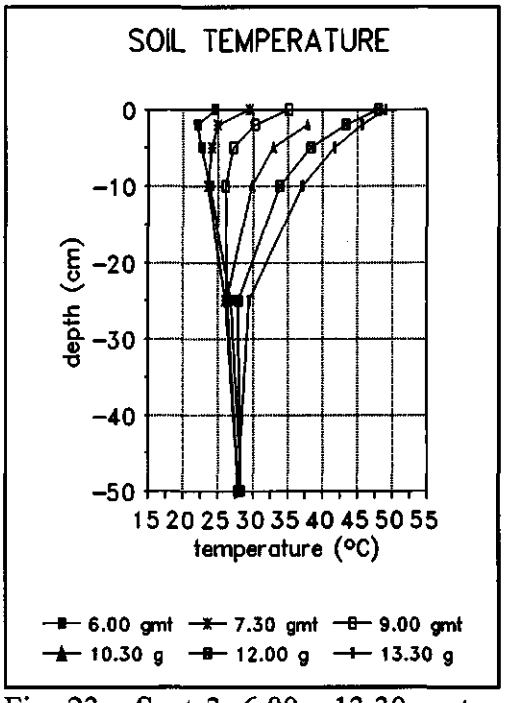

Fig. 23a: Sept 3, 6:00 - 13:30 gmt

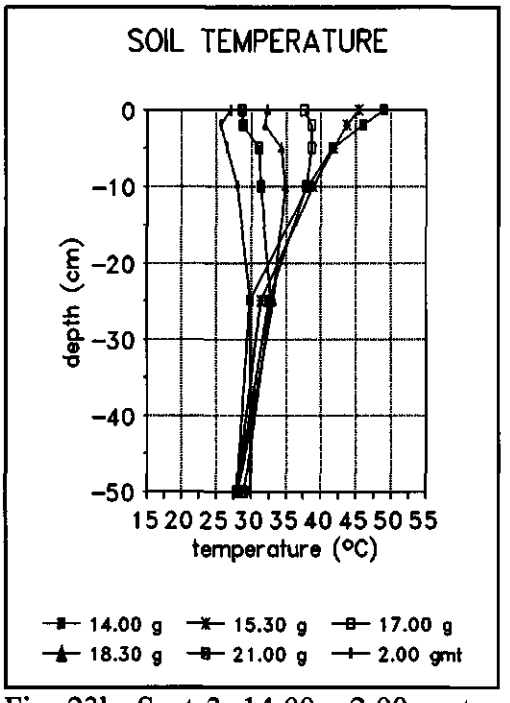

Fig. 23b: Sept 3, 14:00 - 2:00 gmt

Fig. 23: Selected soil temperature profiles from observations of 30 minutes time intervals for one day

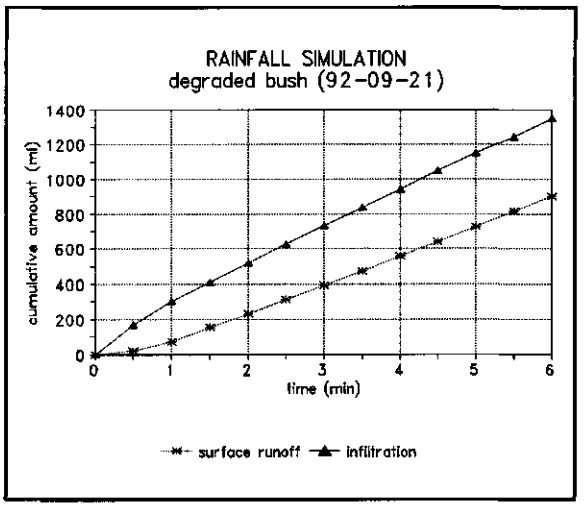

Fig. 24a: slope testplot 5 %

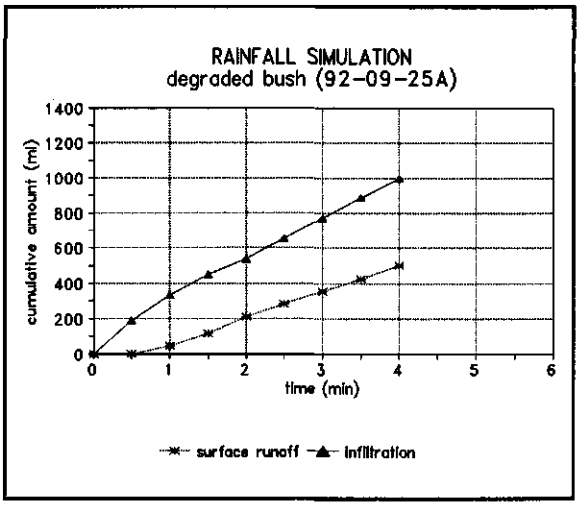

Fig. 24b: slope testplot 2.5 %

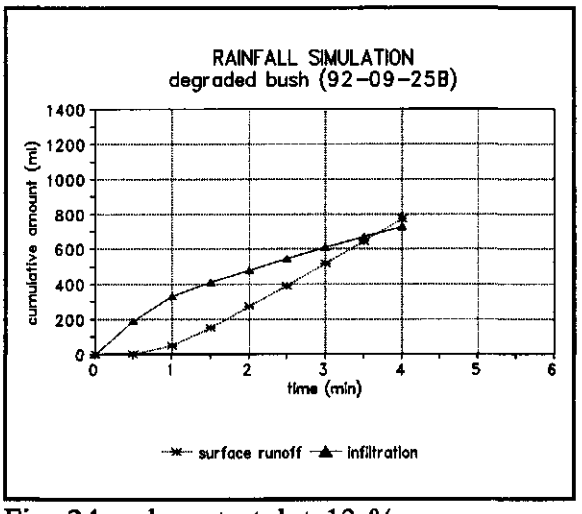

Fig. 24c: slope testplot 13 %

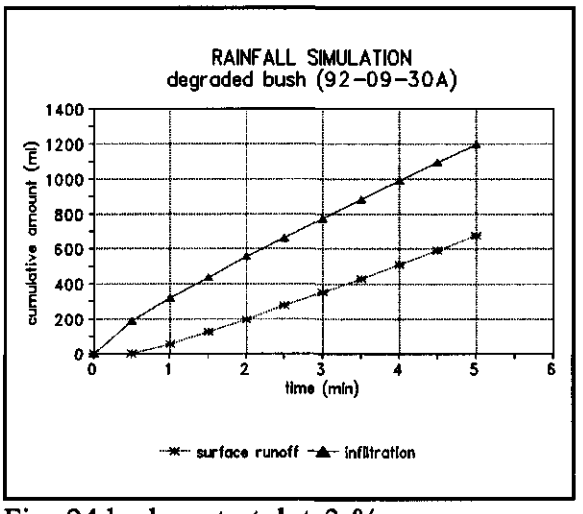

Fig. 24d: slope testplot 3 %

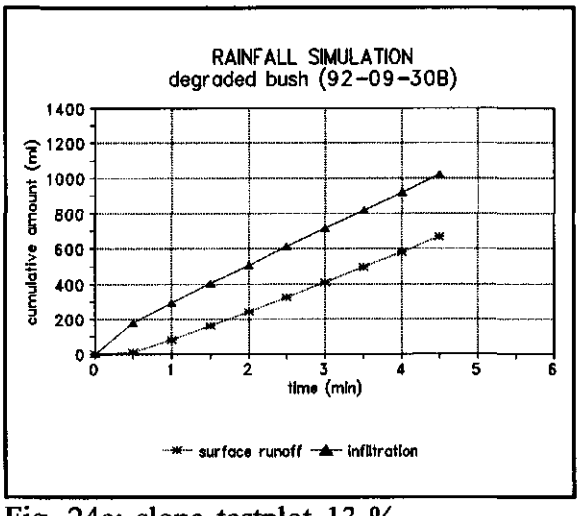

Fig. 24e: slope testplot 13 %

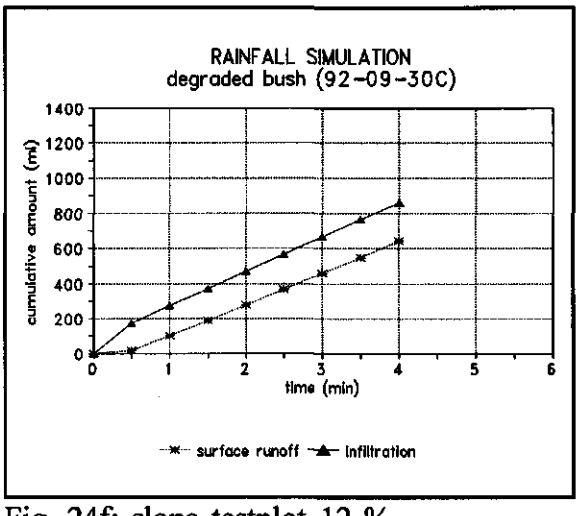

Fig. 24f: slope testplot 12 %

Fig. 24: Cumulative runoff and infiltration by rainfall simulation

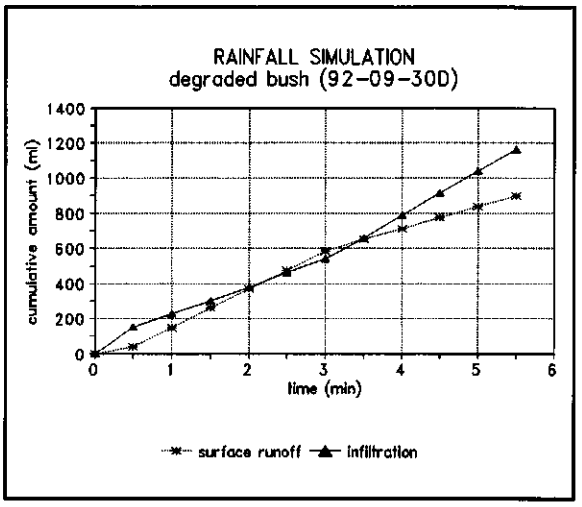

Fig. 24g: slope testplot 17%

Fig. 24: Cumulative runoff and infiltration by rainfall simulation

3.9 SURFACE SOIL MOISTURE

Calibrated moisture contents in the upper soil layer have been stored in the file TDRSURF.DAT. The available data are summarized in Table 7.

Table 7: Measurements of surface soil moisture

subsite	date	time (GMT)	no. of points
fallow bush	92-08-23	starting 13:00	10
millet	92-08-25	11:00 - 12:30	32
degraded bush	92-08-25	starting 13:45	41
	92-09-02	starting 12:30	39
	92-09-12	12:00 - 13:00	41
sparsely covered milletfield	92-08-23	starting 13:30	11
	92-08-25	starting 13:00	49
	92-08-26	11:45 - 13:15	24
	92-09-02	starting 14:30	24
	92-09-12	starting 13:30	24

4 REFERENCES

Ankeny, M.D., M. Ahmed, T.C. Kaspar and R. Horton. 1991. Simple field method for determining unsaturated hydraulic conductivity. Soil Sci. Soc. Am. J. 55: 467-470.

Boast, C.W. and T.M. Robertson. 1982. A "micro-lysimeter" method for determining evaporation from bare soil: description and laboratory evaluation. Soil Sci. Soc. Am. J. 46: 689-696.

Brombacher, A. and L.A.A.J. Eppink. Applications and constraints of the mini-rainfall simulator after Kamphorst. Wageningen Agricultural University, Department of Irrigation and Soil and Water Conservation. In preparation.

Casenave, A. and C. Valentin. 1989. Les etats de surface de la zone sahelienne: influence sur l'infiltration. Orstom, Paris.

Gardner, W.R. 1958. Some steady-state solutions of the unsaturated moisture flow equation with application to evaporation from a water table. Soil Sci. 85: 228-232.

Greacen, E.L. 1981. Soil water assesment by the neutron method. CSIRO, East Melbourne, Australia.

Goutorbe, J.P., T. Lebel, A. Tinga, H. Dolman, E.T. Engman, J.H.C. Cash, P. Kabat, Y.H. Kerr, B. Monteny, S. Prince, P. Sellers, J. Wallace and M. Hoepffner. 1992. Experiment plan for HAPEX-Sahel (second draft). Centre National de Recherches Météorologiques, Toulouse, France.

Heimovara, T.J. and W. Bouten. 1990. A computer controlled 36 channel Time Domain Reflectometry system for monitoring soil water contents. Water Resour. Res. 26: 2311-2316.

Kamphorst, A. 1987. A small rainfall simulator for the determination of soil erodibility. Netherlands Journal of Agricultural Sciences 35: 407-415.

Marthaler, H.P., W. Vogelsanger, F. Richard & P.J. Wierenga. 1983. A pressure transducer for field tensiometers. Soil Sci. Soc. Am. J. 47: 624-627.

Monincx, S. Calibration of the Wallingford neutron probe (nr. 64) for interpretation of measurements in Ouallam (Niger). Wageningen Agricultural University, Department of Water Resources. March 1993.

Reynolds, W.D. and D.E. Elrick. 1991. Determination of hydraulic conductivity using a tension infiltrometer. Soil Sci. Soc. Am. J. 55: 633-639.

Roth, K., R. Schulin, H. Flühler & W. Attinger. 1990. Calibration of Time Domain Reflectometry for water content measurement using a composite dielectric approach. Water Resour. Res. 26: 2267-2273.

Smettem, K.R.J. and B.E. Clothier. 1989. Measuring unsaturated sorptivity and hydraulic conductivity using multiple disc permeameters. J. Soil Sci. 40: 563-568.

Thony, J.L., G. Vachaud, B.E. Clothier and R. Angulo-Jaramillo. 1991. Field measurement of the hydraulic properties of soil. Soil Technology 4: 111-123.

Topp, G.C., J.L. Davis and A.P. Annan, 1980. Electromagnetic determination of soil water content: Measurements in coaxial transmission lines. Water Resour. Res. 16: 574-582.

Van Dam, J.C., J.N.M. Stricker and P. Droogers. 1992. Inverse method for determining soil hydraulic functions from one-step outflow experiments. Soil Sci. Soc. Am. J. 56: 1042-1050.

Van Genuchten, M.Th. 1980. A closed-form equation for predicting the hydraulic conductivity of unsaturated soils. Soil Sci. Soc. Am. J. 44: 892-898.

Wooding, R.A. 1968. Steady infiltration from a shallow circular pond. Water Resour. Res. 4: 1259-1273.

APPENDIX I

GENERAL DESCRIPTION OF SUBSITES AND PLOTS SURROUNDING NEUTRON PROBE ACCESS TUBES

For each plot the following characteristics are described:
- plotnumber (=number of neutron probe access tube)
- number of available photograph(s)
- vegetation
- local slope
- surface characteristics
- local surroundings
- remarks

Abbreviations used for the different characteristics are:

- vegetationtype:	h	herbaceous
	b	bush
	m	millet
	g	grass
- vegetation density:	d	dense vegetation
	o	open vegetation
	n	bare soil, no vegetation
- local slope:	0	flat (0 - 1 à 2%)
	1	slighly sloping (1 à 2% - 3%)
	2	steep (> 5%)

(combinations of codes are possible)

- surface characteristics:	c	surface crust ≈ 100%
	s	sandy surface ≈ 100%
	cs	mainly surface crust
	sc	mainly sandy surface

sandy surface can also imply formation of a crust beneath a thin layer of sand; additional information is given by code l(ight), indicating crust harshness or thickness of the sandy layer

- local surroundings: short description of situation near a plot like no bushes, no millet, access tube in local depression etc.; to be interpreted in combination with photographs

Note that descriptions have been made at the end of August. Important changes in local surroundings of a plot are depicted photographically at the end of the SOP.

FALLOW BUSH AND GRASSLAND

General characterization.
The fallow bush subsite showed an overall mild slope with all kinds of variation on a smaller scale. Microrelief and existence or absence of a surface crust caused a redistribution of precipitation at the surface. The general slope caused partly runoff of precipitation to a depression (∅ ≈ 30 m), where also surface runoff from the sparsely covered millet field was collected. In this depression the water infiltrated relatively fast (within 24 hours).

The grassland was merely flat with some microrelief. In August the vegetation mainly existed of herbaceous vegetation, grasses just started to grow. The soil surface varied continuously (on a scale of decimeters) between a thin sandy layer and a light surface crust.

Plots fallow bush.

plot	photograph	vegetation	slope	surface	number of bushes within radius 2 meter	remarks
21	1,43	h/o	0	sc	0	herbes ≈ 5 cm high
22	2,44	h/o	2	sc	2	access tube ≈ 1 m from large bush
23	3	h/o	1	cs	1	
24	4,45	h/o	0/1	cs	0	clumps of grass
25	5,46	h/o/n	1	cs	1	
26	6	n	1	c	0	harsh, bare spot
27	7,47	h/o	1	sc	2	
28	8	h/o	1	sc	0	
29	9,48	h/o	0/1	sc	1	
30	10	h/o	0/1	sc	1 (small)	30, 31 and 32 situated on local slope and depression
31	11	h/o	1/2	sc	0	
32	12,13,49	0/n	0	cs	1	local depression

Plots grassland.

plot	photograph	vegetation + height	slope	surface	remarks
41	14,50	vo 0-5 cm	0	cs	in slight local depression
42	15,51,	o 5-15 cm	1	sc	slightly higher than surroundings
43	16,52	vo 5-10 cm	0	s	≈ 10 m from large erosion gully
44	17,53	vo 5-10 cm	1/2	sc	

(additional v --> very)

MILLET

General characterization.
Relatively flat area with microrelief. The millet plant was well developed and the field looked better than most fields in the area. However there was still a high variety between well developing parts of the field and poorly covered parts.
The soil surface of the millet subsite could roughly be divided into mainly sandy (≈ 70%), and a mixture of sand and crust.
In case of full grown millet, the distance between plants was 1.2 à 1.0 meter. Roots of millet plants sprawled widely.

Plots millet.

plot	photograph	vegetation	slope	surface	millet in direct surroundings	number of plants within radius 1 meter
1	18,54	m/d	1	s	well developed	3
2	19,55	m/d	0/1	s	very well	1 (big)
3	20,56	m/o	0/1	sc	moderately	1 (small)
4	21,57	m/od	1	s	reasonably well	3 (reasonable)
5	22,58	m/o	1	sc	moderately	2 (small)
6	23,59	m/d	0/1	s	well developed	4 (big)
7	24,60	n	0	sc	badly	0
8	25,61	m/o	1	sc	quite moderate, near area of well developed milletplants	1
9	26,62	n	1	sc	badly	1
10	27,63	m/o	0	s	moderately	2

DEGRADED BUSH

General characterization.
Flat or slightly sloping area. Partly in use as passing route for cattle, causing clearly distinguishable tracks.
Sharp distinction in areas that were not degraded (A-horizont exists) and areas with fully degraded surfaces. The latter parts had no vegetation and were completely covered by surface crusts. The A-horizont was covered by a vegetation of bushes and a low vegetation of Zornia glockidata as monoculture. The area with vegetation had a merely open character.

Plots degraded bush.

plot	photograph	vegetation	slope	surface	surroundings	remarks
51	64	o/d+h	1	c	open+bush	
52	28,29,65	o+h	0	s/lc		
53	30,66	o/n+h	1	c/ls	right next to bush	
54	31	d+h	0	s		
55	32	n (90%)	0	s	change from bare to overgrown surface	
56	33,67	d+h	0	s	surrounded by bushes	
57	34	o+h	0	s/lc	in cattle tracks near bush	
58	35,68	n	0	c	in local depression (pool)	
59	36	h	0	s	on top of local slope	
60	37	n	0	c	in catchment	inundates in case of runoff
61	38,69	n	0	c	in catchment	
62	39	d+h	1	sc	in catchment; at border of open area	
63	40,70	o+h	1	s	in catchment	
64	41,42	o+h	0	sc	in catchment	
	71					temperature profile

APPENDIX II

DATA SETS

file	contents
COUNTRAT.DAT	neutron probe: count ratio
STANDCTS.DAT	neutron probe: standard counts in water
CTSTHETA.DAT	neutron probe: calibrated volumetric moisture content
DIEL.DAT	TDR: measured dielectric constant
DIELCAL.DAT	TDR: calibrated dielectric constant
TDRTHETA.DAT	TDR: calibrated volumetric moisture content
TENSIO.DAT	tensiometer: corrected soil water suction
DISC<date>.DAT	disc permeameter: measurement, started at <date>
MICROLYS.DAT	micro-lysimeters: measured evaporative loss of mass
LYSPROF.DAT	micro-lysimeters: measured moisture profile
TEMPPROF.DAT	temperature profile: calibrated volumetric moisture content and soil temperature
RAINSIM.DAT	rainfall simulation: measured run-off and calculated infiltration
TDRSURF.DAT	TDR: moisture content surface layer

set of photographs

number	description
1-13	fallow bush: (standard)plots at the end of August
14-17	grassland: (standard)plots at the end of August
18-27	millet: (standard)plots at the end of August
28-42	degraded bush: (standard)plots at the end of August
43-49	fallow bush: (standard)plots at the end of the SOP
50-53	grassland: (standard)plots at the end of the SOP
54-63	millet: (standard)plots at the end of the SOP
64-71	degraded bush: (standard)plots at the end of the SOP
72-97	disc permeameter measurements
98-103	fallow bush: sampling transect
104-113	micro-lysimeter spots
114-115	degraded bush: catchment

APPENDIX III

CORRECTED DEPTH NEUTRON PROBE MEASUREMENTS

standard	15	25	35	45	60	75	95	115	135	155	170
corrected											
plot 1	17	27	37	47	62	77	97	117	137	157	172
plot 2	19	29	39	49	64	79	99	119	139	159	174
plot 3	20	30	40	50	65	80	100	120	140	160	180
plot 4	18	28	38	48	63	78	98	118	138	158	173
plot 5	18	28	38	48	63	78	98	118	138	158	173
plot 6	18	28	38	48	63	78	98	118	138	158	173
plot 7	23	33	43	53	68	83	103	123	143	163	178
plot 8	18	28	38	48	63	78	98	118	138	158	173
plot 9	24	34	44	54	69	84	104	124	144	164	179
plot 10	18	28	38	48	63	78	98	118	138	158	173
plot 21	15	25	35	45	60	75	95	115	135	155	170
plot 22	18	28	38	48	63	78	98	118	138	158	
plot 23	21	31	41	51	66	81	101	121	141	161	176
plot 24	18	28	38	48	63	78	98	118	138	158	173
plot 25	17	27	37	47	62	77	97	117	137	157	172
plot 26	16	26	36	46	61	76	96	116	136	156	171
plot 27	17	27	37	47	62	77	97	117	137	157	172
plot 28	18	28	38	48	63	78	98	118	138	158	173
plot 29	19	29	39	49	64	79	99	119	139	159	174
plot 30	20	30	40	50	65	80	100	120	140	160	175
plot 31	20	30	40	50	65	80	100	120	140	160	175
plot 32	19	29	39	49	64	79	99	119	139	159	174
plot 41	19	29	39	49	64	79	99	119	139	159	174

standard	15	25	35	45	60	75	95	115	135	155	170
corrected											
plot 42	20	30	40	50	65	80	100	120	140	160	175
plot 43	21	31	41	51	66	81	101	121	141	161	176
plot 44	18	28	38	48	63	78	98	118	138	158	173
plot 51	26	36	46	56	71	86	106	126			
plot 52	15	25	35	45	60	75	95	115	135	155	170
plot 53	20	30	40	50	65	80	100	120	140	160	
plot 54	17	27	37	47	62	77	97	117	137	157	
plot 55	18	28	38	48	63	78	98	118	138	158	173
plot 56	14	24	34	44	59	74	94	114	134	154	
plot 57	15	25	35	45	60	75	95	115	135	155	
plot 58	20	30	40	50	65	80					
plot 59	15	25	35	45	60	75	95				
plot 60	16	26	36	46	61	76	96				
plot 61	15	25	35	45	60	75					
plot 62	18	28	38	48	63	78					
plot 63	17	27	37	47	62						
plot 64	15	25	35	45	60	75					

APPENDIX IV

DISC PERMEAMETER MEASUREMENTS

file	subsite	crust-type	disc permeameter	surface	subsurface	photograph number	remarks
disc2108	millet	erosion	A	08-21	08-28	72	
disc0109	degraded bush	erosion	A+B	09-01	09-02	73,74	
disc0309	degraded bush	erosion	A+B	09-03		75-77	surface disturbed after refilling reservoir; not measured at subsurface
disc0509	degraded bush	erosion	A	09-05	09-08		disc B damaged
disc0909	E-Central supersite (tigerbush)	gravel	A+B	09-09			intercomparison; not measured at subsurface
disc1009	fallow bush	erosion	A+B	09-10	09-11	78-80	
disc1209	fallow bush	ST3	A+B	09-12	09-13	81,82	
disc1409	degraded bush	ST3	A+B	09-14	09-15	83-85	
disc1709	Northern Satellite site (millet)	---	A+B	09-17		86	no crust; not measured at subsurface
disc1809	Northern Satellite site (millet)	---	A+B	09-18			no crust; not measured at subsurface
disc2009	degraded bush	ST3	A+B	09-20	09-22	87	B at surface: air under supply membrane
disc2109	degraded bush	erosion	A+B	09-21	09-23	88	intercomparison surface-measurement
disc2409	millet	erosion	B	09-24	09-25	89	disc A damaged
disc2609	millet	erosion	A+B	09-26	09-28		
disc2909	fallow bush	erosion and ST3	A+B	09-29	09-30	90-92	
disc0110	tigerbush	ST3	A	10-01	10-02	93	disc A damaged
disc0310	tigerbush	ST3	A	10-03			disc A damaged; not measured at subsurface
disc0410	tigerbush	ST3	A+B	10-04		94	not measured at subsurface
disc0510	tigerbush	algea	A+B	10-05		95,96	not measured at subsurface
disc0610	tigerbush	algea	A+B	10-06		97	not measured at subsurface

APPENDIX V

SAMPLING SOIL HYDRAULIC PROPERTIES

FALLOW BUSH

I sampling near plots (distance ≈2 m)

plot	volume (cm^3)	depth (cm)
21	100	10-15
	100	35-40
22	100	10-15
	100	35-40
23	100	10-15
	100	35-40
24	100	10-15
	100	35-40
25	100	10-15
	100	35-40
26	100	10-15
	100	35-40
27	100	10-15
	100	35-40
28	100	10-15
	100	35-40
29	100	10-15
	100	35-40
30	100	10-15
	100	20-25
	100	30-35
	100	37-42
	100	45-50
	100	55-60

II sampling transect:
- Open area between bushes.
- Approximately 7 meters South-West of plot 25.
- Length approximately 11 meters.
- Sampling repetition each 1.1 meter (10 parts).
- Transect has declining slope from part 1 to 10.
- Vegetation: herbaceous and grasses; no erosion.
- Sampling: 100 cc and 250 cc at a depth of 10-15 cm, 600 cc at a depth of 10-22 cm; at a distance of 30 cm (from starting point of each part) 100 cc, at 55 cm 250 cc and at 80 cm 600 cc.
- See also photographs.

part	volume (cc)	depth (cm)
7	100	8-13
	100	21-26
	600	20-32
8	100	7-12
	100	21-26
	600	21-33
9	100	6-11
	100	21-26
	600	20-32
10	100	7-12
	100	21-26
	600	22-34

NORTHERN SATELLITE SITE (See Fig. 20)

sampling transect no.	volume (cm^3)	depth (cm)	vegetation
100	250	10-15	millet
200	250	10-15	millet
	100	30-35	
300	250	10-15	trees and bushes
500	250	10-15	trees and bushes
	100	30-35	
700	250	10-15	1st year fallow
	100	30-35	
800	250	10-15	2nd year fallow
900	250	10-15	2nd year fallow
	100	30-35	
1000	250	10-15	2nd year fallow
1160	250	10-15	2nd year fallow
	100	30-35	

number = distance from meteo-mast of 'Copenhagen'-group

MILLET

sampling near plots (distance ≈ 2 m)

plot	volume (cm^3)	depth (cm)
1	100	10-15
	100	35-40
	100	25-30
2	100	10-15
	100	35-40
3	100	10-15
	100	35-40
4	100	10-15
	100	35-40
5	100	10-15
	100	35-40
6	100	10-15
	100	35-40
7	100	10-15
	100	35-40
8	100	10-15
	100	35-40
9	100	10-15
	100	35-40

DEGRADED BUSH

sampling transect
- Length transect approximately 10 meters in East-West direction.
- Approximately 30 meters South-West of the flume.
- Transect part 1-5: fully eroded, no A-horizont; transect part 6-10: A-horizont 0-15 cm depth.

part	volume (cm^3)	depth (cm)
1	100	10-15
	600	15-27
2	100	10-15
	600	15-27
3	100	10-15
	600	15-27
4	100	10-15
	600	10-22
5	100	10-15
	600	10-22
6	100	7-12
	100	20-25
	600	20-32

APPENDIX VI

LOCATIONS OF MICRO-LYSIMETER SPOTS

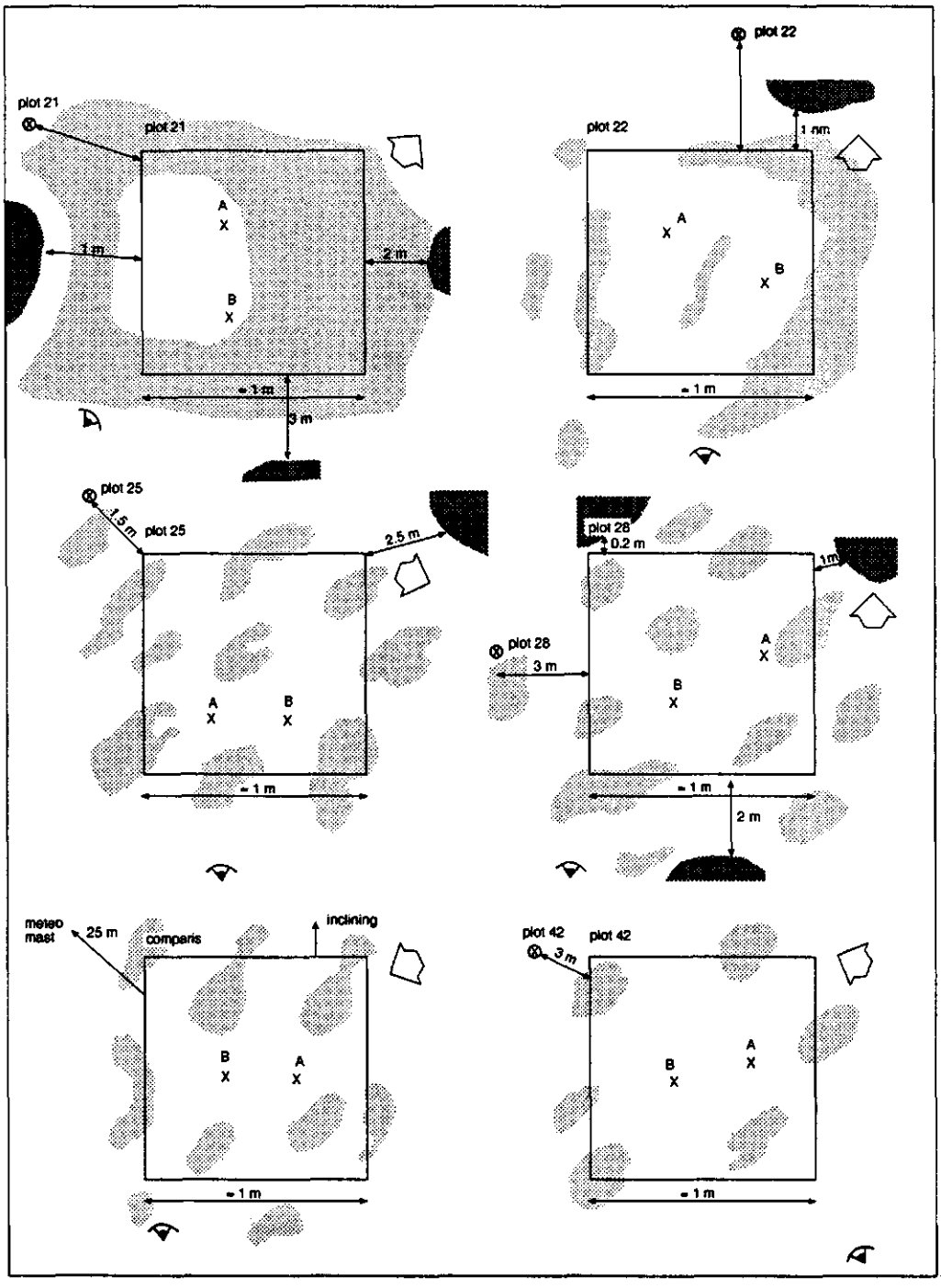

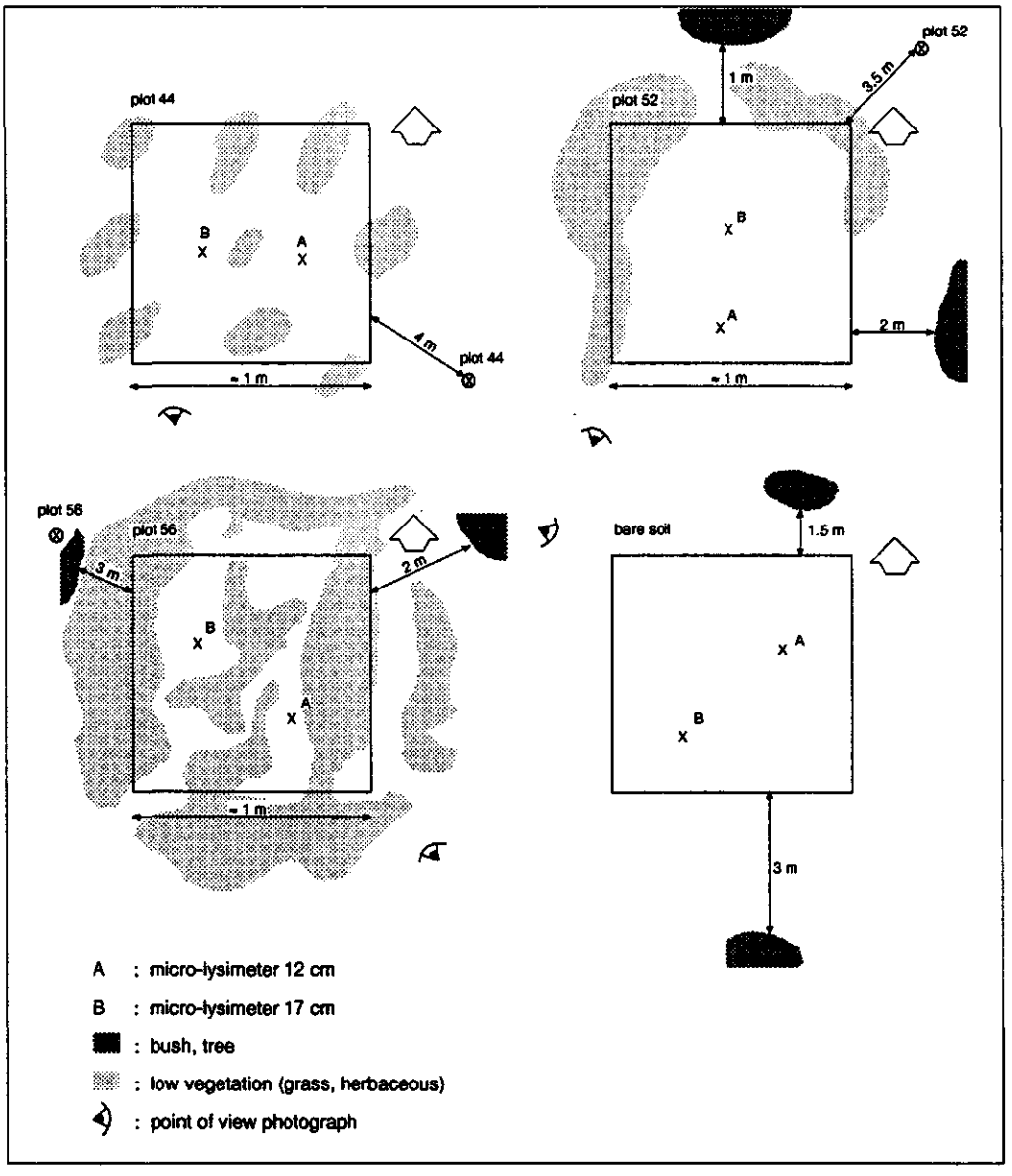
plot 44
B
A
4 m
plot 44
≈ 1 m
plot 52
1 m
3.5 m
plot 52
B
A
2 m
≈ 1 m
plot 56
plot 56
3 m
2 m
B
A
≈ 1 m
bare soil
1.5 m
A
B
3 m
A : micro-lysimeter 12 cm
B : micro-lysimeter 17 cm
: bush, tree
: low vegetation (grass, herbaceous)
: point of view photograph